Plasticity Model for Partially Prestressed Concrete

Milad Hafezolghorani[1], Farzad Hejazi[1]*, Mohd Saleh Jaffar[1] and Hojjat Adeli[2]

[1]*Department of Civil Engineering, University Putra Malaysia, Malaysia*

[2]*Faculty of Engineering, Ohio State University, Columbus, USA*

*Corresponding author, Email: farzad@upm.edu.my

Abstract

Recently, the partially prestressed concrete (PPC) has been widely used as an effective construction technique for structures to reduce yielding and damages. However, there is no proper analytical model for PPC frame elements (beam-column members) to perform the finite element analysis. Besides, an extensive review of the literature uncovered little available information about the possibility of identifying damage to PPC members during applied vibration loads such as earthquake excitation. Hence, this paper presents the development of a new 3D analytical model for PPC beam-column element subjected to static and dynamic loads. In addition, a theory of plasticity and yielding surfaces for PPC frame elements are formulated in order to detect damage and determine the location of plastic hinges in the structural components under dynamic load. The developed analytical and plasticity models were codified and implemented in a finite element program in order to perform inelastic static and dynamic analysis for PPC structures. Then, sample PPC beam and frame members were cast and tested experimentally for flexural and incremental loading, respectively, to verify the developed analytical and plasticity model for PPC. The results show a good agreement between the analytical model and numerical analysis and the experimental test results. In addition, a comparison of the seismic response of reinforced concrete (RC) and PPC structures indicated that the stiffness and energy dissipation capacity of the structure with PPC members improved noticeably and the total number of plastic hinge formations in the structural members decreased.

Keywords: Prestressed concrete, damage plasticity, analytical model, plasticity model, finite element, stiffness, energy dissipation

1. INTRODUCTION

Prestressing concrete was introduced in the early 1940s to overcome the natural weakness of concrete in tension. The term “partially prestressed element” normally implies combining the conventional reinforcing steels and prestressing steel strands to strengthen a flexural concrete member.

Naaman (1983) proposed an approximate nonlinear analysis technique to simulate the ultimate behavior of fully prestressed concrete (FPC) and PPC beams. Using a nonlinear programming approach, Cohn and MacRae (1984) compared the optimization results for 240 RC, FPC and PPC beams. Naaman et al. (1986) compared experimental data with a proposed nonlinear analytical model to evaluate the flexural ductility of PPC elements under static loading. Skogman et al. (1988) developed a computer program based on an iterative strain compatibility method to analyze the flexural strength of PPC members. Shushkewich (1990) presented a simple mathematical model to determine the stresses of uncracked or cracked PPC structural elements. Chern et al. (1992) used bending theory to analyze the behavior of PPC members. Alkhairi and Naaman (1993) developed a nonlinear analytic model to investigate the moment-deformation response of bonded and unbonded PPC members. Gupta et al. (1994) proposed an object-oriented approach (Yu and Adeli, 1993; Hung and Adeli, 1994) for detecting damage~~s~~ in prestressed concrete bridges. Sarma and Adeli (1998) presented a review of methods for cost optimization of concrete structures. Tanchan (2001) conducted an experimental study to investigate the behavior of nine FPC high-strength concrete (HSC) beams that had been prestressed with unbonded tendons up to failure. Ariyawardena and Ghali (2002) presented a numerical method to predict the behavior of concrete structures prestressed with internal or external tendons throughout their loading history. Au and Du, (2004) reviewed the methods to evaluate the performance of PPC members with bonded and unbonded steel tendons and fiber-reinforced polymer.

Recupero et al. (2005) proposed an analytical model to investigate the performance of FPC beams subjected to the interactions of bending moments and shear force; the interaction of axial forces, biaxial bending moments, or shear forces was not taken into account to develop a comprehensive damage theory. The developed damage theory was not able to identify the plastic hinge formations. Sirca and Adeli (2005) presented a model for cost optimization of prestressed concrete bridges.

Franchetti et al. (2009) experimentally investigated the static and dynamic responses of three precast prestressed concrete beams and proposed a damage detection method based on free vibration tests and nonlinear damping identification. Lou et al. (2013) described a numerically-based finite element model to estimate the total nonlinear response of continuous concrete beams prestressed with internal unbonded tendons. Karayannis and Chalioris, (2013) proposed a design process for PPC beams based on the cracking control provisions by adopting a design maximum allowable crack width.Serviceability and ductility of partially prestressed concrete beams under limited cycles of repeated loading were investigated by Oukaili and Khattab (2019). Application of partial prestressing for crack control in reinforced concrete structures was investigated by Choudhary and Akhtar (2019) and Xue et al. (2020).

A number of researchers have presented new approaches for damage detection and health monitoring of both concrete and steel structures (Sirca and Adeli, 2012; Amezquita-Sanchez and Adeli, 2016). Qarib and Adeli, (2014) and Lei et al., (2015) developed algorithms for the identification and damage detection in structures under severe loading using the stiffness degradation of structural members. Zhang et al. (2019) presented a novel computer-vision and deep-learning techniques to effectively detect cracks in structural infrastructure under various conditions. Li et al. (2019) proposed a fully convolutional network (FCN)-based multiple damages detection method for concrete structure.

Several researchers (Ayoub and Filippou, 2009; Laskar et al., 2010) have implemented the nonlinear models to evaluate the performance of PPC structure using commercial FE packages. Navarro et al. (2007) proposed a general 3D model to analyze RC and FPC frame elements without identifying the damaged areas. Ozkul (2007) presented a general approach for the analysis of concrete beams prestressed with unbonded tendons, using the commercial, general purpose finite element commercial software. Huang (2012) investigated possible approaches for modeling of FPC structures and the interface between the concrete and prestressing tendons, using the finite element commercial software. Preciado et al. (2016) investigated the effect of external prestressing medieval and masonry bell towers subjected to strong earthquakes using the commercial software. However, modeling a simple prestressed element using FEM commercial software requires extensive experience and high computation time, which increase the cost of design and analysis (Al-Jurmaa and Abdul-Razzak, 2009). Also, a review of the literature reveals insufficient available experimental tests data to verify

and validate the structural performance of PPC beams and frame buildings under static and dynamic loads considering the plastic hinge formation mechanism (Kien, 2008).

Thanoon et al. (2004) identified the major difficulties encountered in inelastic analysis of a RC frame as distribution of inelastic stiffness along the member length and inelastic stiffness of the member changing continuously with stress history. They developed an analytical model for a two-node RC beam-column element consisting of two plastic hinges at the ends of the element was developed. Spinella (2013) proposed analytical moment-curvature interaction diagrams by considering nonlinear constitutive laws to evaluate the failure mechanism of arbitrarily shaped RC sections under biaxial bending moments and axial force. Talaeitaba and Torki (2014) developed a nonlinear finite element model to assess the effect of transverse reinforcement on the shape of the shear-torsion interaction curve of RC beams and presented a plasticity theory to detect damage in RC members due to shear and torsion. Hejazi et al. (2013, 2014, and 2016) developed new analytical model for inelastic dynamic analysis of RC framed structures and detected the plastic hinges during applied seismic excitation. Tang and Chen (2019) carried out experimental and numerical investigations on the plain concrete in beams subjected to three-point bending. ESPI technique was used to observe crack evolution and measure the full-field deformation of the beams.

As presented in this brief review, considerable effort has been expended to develop analytical and numerical methods to study the nonlinear behavior of RC building structures. However, the analysis of PPC members is more complicated compared to the analysis of conventional RC members, due to the presence of bonded and unbonded prestressing strands and corresponding forces. Hence, a comprehensive three-dimensional (3D) analytical model associated with a failure criteria theory (yielding mechanism) to determine the damaged areas in PPC structures under dynamic loads is required to evaluate the seismic performance of structures with PPC members. Since, available commercial software packages do not provide a special PPC frame element with possibility of yielding and crack detection in member, modeling and analysis of complicated PPC structures under seismic excitations remains challenging.

This paper presents the development of an analytical and plasticity model for 3D nonlinear PPC frame elements. The model was implemented in a FEM computer program (Fortran programming language) to perform inelastic static and dynamic analyses for PPC structures.

Validation of the analytical and plasticity models was accomplished by conducting experimental test on PPC beams and frame and compare the results of the numerical analysis and experimental testing. Furthermore, the experimental results of a four story PPC building under earthquake excitation tested by Wei et al. (2012) is used to compare and validate the developed analytical model.

2. ANALYTICAL MODEL FOR PPC FRAME ELEMENT

2.1 Schematic Design of the Member and Constitutive Relationship

The PPC technique enhances the capacity of concrete members and decreases the yielding and damage (crack) in structures, thus providing an alternative to the conventional RC and FPC techniques. However, predicting the response of structures with PPC members subjected to the static and dynamic loading involves many complexities, which arise from the presence of bonded and unbonded prestressing strands and corresponding forces, as well as the interaction between the concrete and the strands. Hence, a particular 3D FE-based analytical model for the PPC frame element is presented in this paper.

The schematic design and the associated degrees of freedom (DOFs) for PPC member considered in this study are shown in Figure 1. The PPC frame element is represented by two rigid block zones which represent the joint at ends of element; two 3D plastic hinges (assumed to have zero length) reflect the member's inelastic behavior; and an elastic part located between two plastic hinges which reflects elastic behavior (Hejazi et al., 2016). To simplify the analytical expressions, the perfect bond assumption is considered for the present model. Appropriate stress-strain relations for the materials are needed to be considered in order to formulate the constitutive law and develop the plasticity and yielding surface model for PPC frame elements. Different mathematical expressions have been suggested in the literature to reflect the physical properties of concrete, reinforcing steel, and prestressing strands.

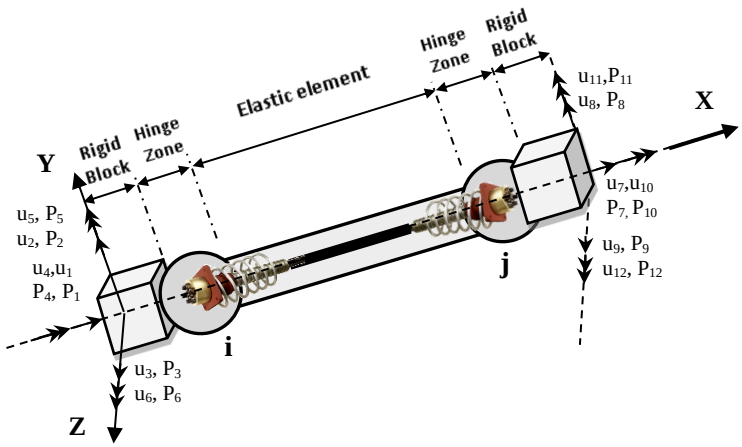

Fig. 1. Three-dimensional analytical model of PPC frame element

The stress-strain relation for concrete in compression initially proposed by Medland and Taylor (1971) has been used by many researchers recently (Thanoon et al., 2004; Hejazi et al. 2013). The relationship between stress (f_c) and strain (ε_c) in concrete is expressed by a unique continuous fourth degree polynomial, applied for both the hardening and softening condition as follows (Medland and Taylor 1971) (Figure2a):

$$f_c = 0.85 f_c'(A\varepsilon_c^4 + B\varepsilon_c^3 + C\varepsilon_c^2 + D\varepsilon_c) \tag{1}$$

where *A*,*B*, *C*, and *D* are the constants of the polynomial and f_c' represents the ultimate compressive strength of concrete. Figures 2b and 2c represent the common idealized constitutive models (elasto-plastic curves) for ordinary reinforcing bars and prestressing strands, respectively (Agrawal and Bhattacharya, 2010). Hence, the relation between stress and strain for non-prestressed steel (f_{st}, ε_{st}) and prestressed strands ($f_p, \varepsilon_p^{total}$) can be presented as follows:

Elastic state;

$$\begin{cases} f_{st} = E_s \varepsilon_{st}\,; & if \quad \varepsilon_{st} \le \varepsilon_{yst} \quad (2) \\ f_p = E_p \varepsilon_p^{total}\,; & if \quad \varepsilon_p^{total} \le \varepsilon_{yp} \quad (3) \end{cases}$$

Elasto-plastic state;

$$\begin{cases} f_{st} = f_{yst} + E_{st}(\varepsilon_{st} - \varepsilon_{yst})\,; & if \quad \varepsilon_{st} > \varepsilon_{yst} \quad (4) \\ f_p = f_{yp} + E_{pt}(\varepsilon_p^{total} - \varepsilon_{yp})\,; & if \quad \varepsilon_p^{total} > \varepsilon_{yp} \quad (5) \end{cases}$$

where the subscripts 'st' and 'p' denote the contributions due to reinforcing steel and prestressing steel rows, respectively. The terms E and E_t are the modulus of elasticity and the slope of the strain-hardening portion of the stress-strain curves, respectively; f_y and ε_y denote the yield stress and yield strain of steel materials, and ε_{yst} and ε_{yp} are equal to f_{yst}/E_s and f_{yp}/E_p, respectively.

2.2. Formulation of the PPC frame element considering combined action of axial force and bending moments

In order to detect damages (yielding points) and determine the location of plastic hinges in inelastic analysis of the PPC elements, a computational scheme based on lumped plasticity model is formulated to present two and three dimensional yield surfaces.

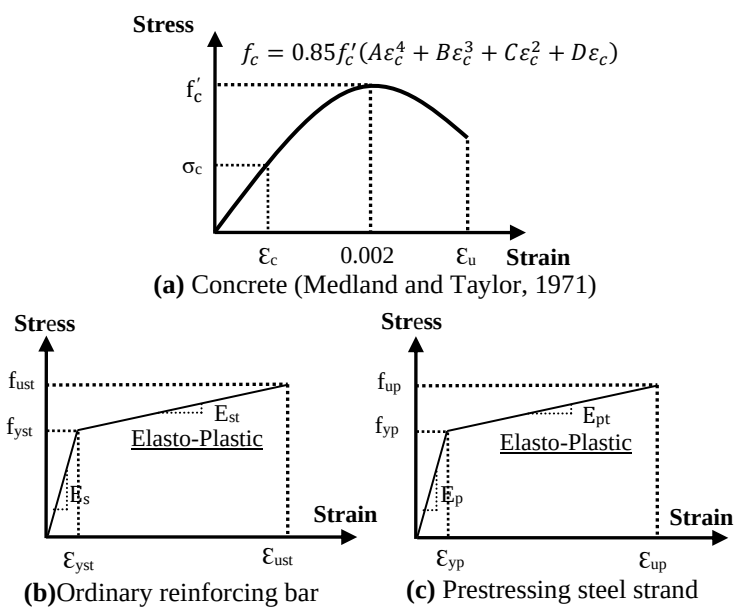

Fig. 2. Stress-strain curves for materials in a PPC member

A plastic hinge is formed at a section when the axial force and bending moment state (p_u,m_u) in the section lie either outside or on the yield surface resulting from the plasticity model. To develop a comprehensive plasticity model, it is necessary to consider the equilibrium of forces and the compatibility of the strains. Figure 3 presents the sectional geometry and possible strain distributions of a PPC member subjected to an applied axial load (P)

and bending moment (M). Subscripts 'i' and 'j' vary from 1 to n, and 1 to m, respectively, where n, and m denote the total number of reinforcing steel and prestressing strand rows in the PPC section, respectively, starting from the bottom to the top of the compression zone (Figure 3a). The total cross-sectional area of non-prestressed steel in the ith layer is $A_{st(i)}$ and the total cross-sectional area of prestressing strands in the jth layer is $A_{p(j)}$. As seen in Figure 3b and c, the terms ε_t and ε_b denote the strains at the outermost top (compression) and bottom (tensile or least compression) edges, respectively. In Figures 3a and 3b, the curvature χ is formulated as:

$$\chi = \frac{\varepsilon_t + \varepsilon_b}{d} = \frac{\varepsilon_t}{kd} = \frac{\varepsilon_c}{y} = \frac{\varepsilon_{st(i)}}{(k-\alpha_i)d} = \frac{\varepsilon_{p(j)}}{(k-\beta_j)d} \tag{6}$$

where d is the section depth; ε_c is the strain in concrete at y distance from the neutral axis; $\varepsilon_{st\,(i)}$ is the strain in the i^t layer of steel; $\varepsilon_{p\,(j)}$ is the strain in the jth layer of the tendon; kd is the neutral axis depth; $\alpha_i d$ is distance of the ith steel layer from the top fiber; and $\beta_j d$ is the distance of jth tendon layer from the top fiber. Defining non-dimensional axial load, bending moment, and curvature as $p = \frac{P}{bdf_c'}, m = \frac{M}{bd^2 f_c'}$ and $\phi = \chi d$, the equilibrium equations for the PPC section (Figure 3a) are derived:

$$p = p_{cn} + p_{st} + p_p \tag{7}$$

$$m = m_{cn} + m_{st} + m_p - \left(p \times \left(\frac{\varepsilon_t}{\phi} - 0.5\right)\right) \qquad \begin{cases} \phi = \phi_{st} & if \quad \beta_m \le \alpha_n \\ \phi = \phi_p & if \quad \beta_m > \alpha_n \end{cases} \tag{8}$$

where the subscripts 'cn', 'st' and 'p' denote the contribution made by the concrete in compression, rows of the reinforcing steels, and bonded prestressing strands, respectively. A perfect bonding between the interfaces of steel, tendon, and concrete is considered in this research. Tensile strength of concrete is neglected in this study and tensile forces due to the external forces in the concrete sections are transferred to the tensile steels and strands. In a 2D analysis, the yield surface is mostly presented by ultimate axial force-moment curve (Hejazi et al., 2013). Figure 4 shows the axial force-bending moment interaction curve (m_u,p_u) and its key points for the PPC section. Line OB in this figure separates the compression and tension regions of the PPC beam-column section. Points 'A' and 'D' represent the ultimate axial compressive p_0 and tensile p_t loads, respectively, defined using theory of strains compatibility and forces equilibrium acting on the PPC cross-section as:

$$p_0 = 1 + \frac{\rho_{st}(f_{yst} - f_c')}{f_c'} + \frac{\rho_p(f_{yp} - f_c')}{f_c'} - \frac{P_{effct}}{bdf_C'} \tag{9}$$

$$p_t = \frac{f_{yst}\rho_{st}}{f_C'} + \frac{f_{yp}\rho_p}{f_C'} \tag{10}$$

where ρ_{st}, ρ_p, and P_{effct} are the total reinforcing steel ratio, prestressing strand ratio, and the total effective prestress force, respectively, defined as follows:

$$\rho_{st} = \sum_{i=1}^{n} \frac{A_{st(i)}}{bd} = \frac{A_{st}}{bd} \tag{11}$$

$$\rho_p = \sum_{j=1}^{m} \frac{A_{p(j)}}{bd} = \frac{A_p}{bd} \tag{12}$$

$$P_{effct} = \sum_{j=1}^{m} P_{effct(j)} \tag{13}$$

where $P_{effct(j)}$ is the effective prestress force in the jth row of the prestressing strand layer.

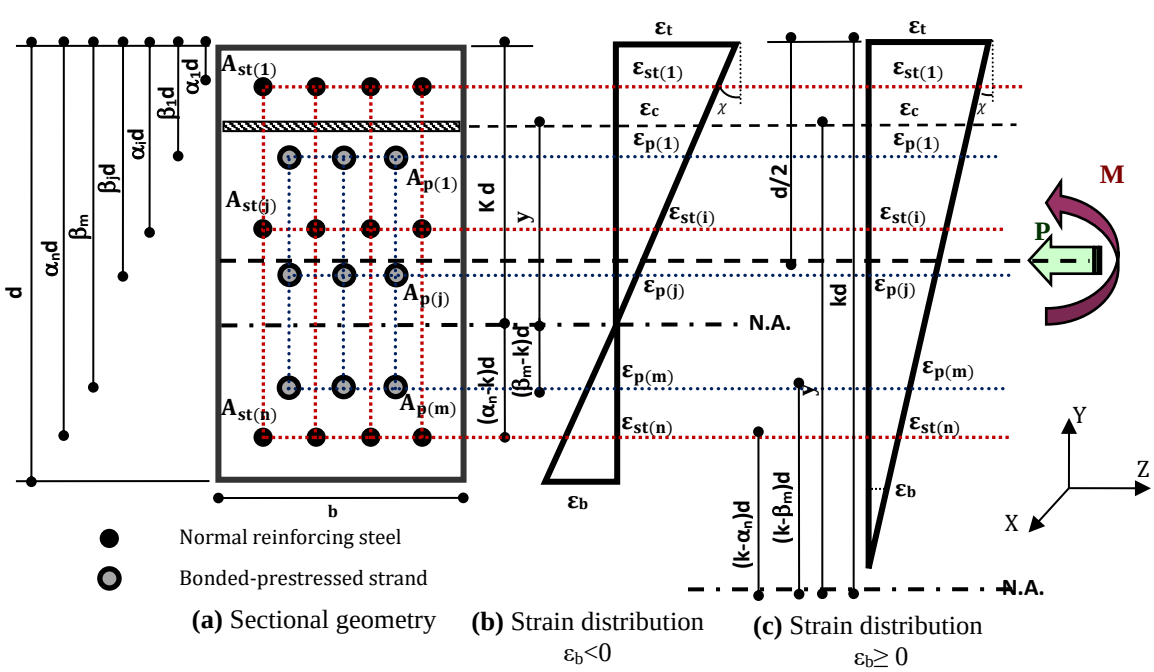

(a) Sectional geometry **(b)** Strain distribution $\varepsilon_b<0$ **(c)** Strain distribution $\varepsilon_b \geq 0$

Fig. 3. Sectional geometry and possible strain distributions of PPC member

Point B represents the balanced condition, and the balanced axial load (p_{ub}) is the applied force when the outermost fiber strain of concrete attains its ultimate compression strain ($\varepsilon_t = \varepsilon_{cu}$) and the last layer of tensile non-prestressed or prestressed steel yields.

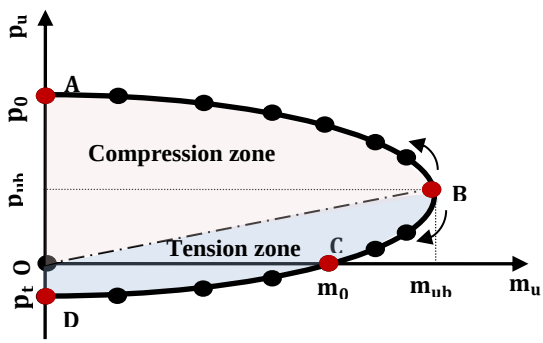

Fig. 4. Axial force-bending moment curve (m_u,p_u)

It should be highlighted that in the balanced condition, the outermost bottom fiber is always in the tension ($\varepsilon_b < 0$), as seen in Figure 3b. The computation procedure for finding the balanced axial load (p_{ub}) and the corresponding moment (m_{ub}) in a PPC section can be written as (Thanoon et al., 2004):

$$\mathrm{p_{ub}} = (p_{cn})_b + (p_{st})_b + (p_p)_b \tag{14}$$

$$\mathrm{m_{ub}} = (m_{cn})_b + (m_{st})_b + (m_p)_b - \left(\mathrm{p_{ub}} \times \left(\frac{\varepsilon_t}{\emptyset_b} - 0.5\right)\right) \tag{15}$$

Derivation of the balanced condition is obtained by substituting the contributions of concrete in compression, reinforcing steel, and prestressed steel strands (tendons) as follows:

$$\mathrm{p_{ub}} = \overbrace{\frac{1}{\emptyset_b}\int_0^{\varepsilon_t} (A\,\varepsilon_c^4 + B\;\varepsilon_c^3 + C\,\varepsilon_c^2 + D\,\varepsilon_c)\,d\varepsilon_c}^{\text{Force due to concrete}} + \overbrace{\sum_{i=1}^{n} \rho_{st(i)} \frac{f_{st(i)}}{f_c'}}^{\text{Force due to reinforcement}} + \overbrace{\sum_{j=1}^{m} \rho_{p(j)} \frac{f_{p(j)}}{f_c'}}^{\text{Force due to prestressing tendons}} \tag{16}$$

$$\mathrm{m_{ub}} = \frac{1}{(\emptyset_b)^2}\int_0^{\varepsilon_t} (A\,\varepsilon_c^5 + B\;\varepsilon_c^4 + C\,\varepsilon_c^3 + D\,\varepsilon_c^2)\,d\varepsilon_c + \frac{1}{(\emptyset_{st})_b}\sum_{i=1}^{n} \rho_{st(i)} \frac{\varepsilon_{st(i)} f_{st(i)}}{f_c'} + \frac{1}{(\emptyset_p)_b}\sum_{j=1}^{m} \rho_{p(j)} \frac{\varepsilon_{p(j)}^{total} f_{p(j)}}{f_c'} - \mathrm{p_{ub}} \times \left(\frac{\varepsilon_t}{\emptyset_b} - 0.5\right) \tag{17}$$

Accordingly, by integration of the equations (16) and (17) over the compressive area of the PPC section, the balanced axial load and the corresponding moment are obtained as follows:

$$\mathrm{p_{ub}} = \frac{1}{\emptyset_b}\left(A\ \frac{\varepsilon_t^5}{5} + B\ \frac{\varepsilon_t^4}{4} + C\ \frac{\varepsilon_t^3}{3} + D\ \frac{\varepsilon_t^2}{2}\right) + \sum_{i=1}^{n} \rho_{st(i)} \frac{f_{st(i)}}{f_c'} + \sum_{j=1}^{m} \rho_{p(j)} \frac{f_{p(j)}}{f_c'} \tag{18}$$

$$\mathrm{m_{ub}} = \frac{1}{(\emptyset_b)^2}\left(A\ \frac{\varepsilon_t^6}{6} + B\ \frac{\varepsilon_t^5}{5} + C\ \frac{\varepsilon_t^4}{4} + D\ \frac{\varepsilon_t^3}{3}\right) + \frac{1}{(\emptyset_{st})_b}\sum_{i=1}^{n} \rho_{st(i)} \frac{\varepsilon_{st(i)} f_{st(i)}}{f_c'} + \frac{1}{(\emptyset_p)_b}\sum_{j=1}^{m} \rho_{p(j)} \frac{\varepsilon_{p(j)}^{total} f_{p(j)}}{f_c'}$$

$$-\left[\frac{1}{\emptyset_b}\left(A\ \frac{\varepsilon_t^5}{5} + B\ \frac{\varepsilon_t^4}{4} + C\ \frac{\varepsilon_t^3}{3} + D\ \frac{\varepsilon_t^2}{2}\right) + \sum_{i=1}^{n} \rho_{st(i)} \frac{f_{st(i)}}{f_c'} + \sum_{j=1}^{m} \rho_{p(j)} \frac{f_{p(j)}}{f_c'}\right] \times \left(\frac{\varepsilon_t}{\emptyset_b} - 0.5\right) \tag{19}$$

where $(\emptyset_{st})_b$ and $(\emptyset_p)_b$ are non-dimensional balanced curvatures (length of ARC over radius of curvature when the outermost fiber strain of concrete attains its ultimate compression strain and the last layer of tensile steel yields simultaneously, as shown in Figure 3) due to the nth and m^{th} layers of reinforcing steel and prestressing strands, respectively, which calculated as:

$$\begin{aligned} \emptyset_b = (\emptyset_{st})_b &= \frac{\varepsilon_t + |\varepsilon_{yst}|}{\alpha_n}\ ; \quad if \qquad \beta_m < \alpha_n \\ \emptyset_b = (\emptyset_p)_b &= \frac{\varepsilon_t + |\varepsilon_{yp}|}{\beta_m}\ ; \quad if\, \beta_m > \alpha_n \end{aligned} \tag{20}$$

In this research, $\varepsilon_{st(i)}$ and $\varepsilon_{p(j)}^{total}$ are the ultimate strains in the nth and m^{th} layers of reinforced steel and prestressed strands, respectively. These values are obtained using the following equations:

$$\varepsilon_{st(i)} = \varepsilon_t - \alpha_i (\emptyset_{st})_b \tag{21}$$

$$\varepsilon_{p(j)}^{total} = \varepsilon_{p(j)} + \varepsilon_{pe(j)} + \varepsilon_{ce(j)} \tag{22}$$

where $\varepsilon_{p(j)}$, $\varepsilon_{pe(j)}$, and $\varepsilon_{ce(j)}$ are the strains in tendons due to flexure, effective pre-strain in tendons, and effective pre-strain in concrete at the jth layer of prestressing tendon, respectively, as shown in Figure 5. The relatively small value of $\varepsilon_{ce(j)}$ is neglected in the current study. Therefore, $\varepsilon_{p(j)}^{total}$ can be written as:

$$\varepsilon_{p(j)}^{total} = \left(\varepsilon_t - \beta_j (\emptyset_p)_b\right) + \frac{P_{effct(j)}}{A_{p(j)} E_p} \tag{23}$$

As observed in Figure 4, point C represents the ultimate moment capacity (m_0) of the PPC frame element when axial force is equal to zero. Since the value of $\emptyset_{st}$ for the ultimate capacity condition is unknown, a trial value of $\emptyset_{st} = \varepsilon_t$ is assumed, and the axial load, (p_c) is calculated using following equations:

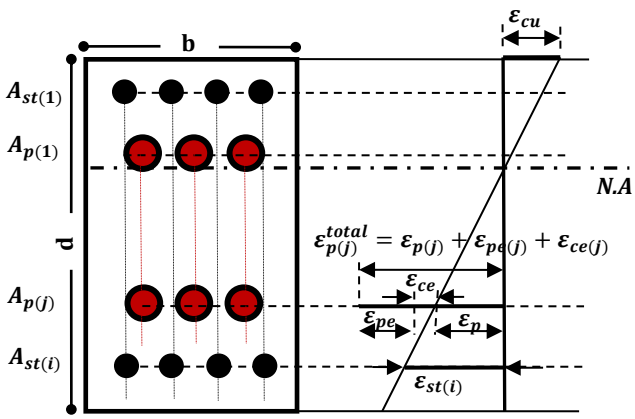

(a) PPC cross-section (b) Strain distribution diagram

Fig. 5. Components of strains in prestressing strand

$$p_c = \frac{1}{\emptyset_{\text{st}}}\left(A\,\frac{\varepsilon_t^5}{5} + B\,\frac{\varepsilon_t^4}{4} + C\,\frac{\varepsilon_t^3}{3} + D\,\frac{\varepsilon_t^2}{2}\right) + \sum_{i=1}^{n}\rho_{st(i)}\frac{f_{st(i)}}{f_c'} + \sum_{j=1}^{m}\rho_{p(j)}\frac{f_{p(j)}}{f_c'}; \qquad if \quad \varepsilon_b \le 0 \tag{24}$$

$$p_c = \frac{1}{\emptyset_{\text{st}}}\left[\frac{A}{5}(\varepsilon_t^5 - \varepsilon_b^5) + \frac{B}{4}(\varepsilon_t^4 - \varepsilon_b^4) + \frac{C}{3}(\varepsilon_t^3 - \varepsilon_b^3) + \frac{D}{2}(\varepsilon_t^2 - \varepsilon_b^2)\right] + \sum_{i=1}^{n}\rho_{st(i)}\frac{f_{st(i)}}{f_c'} + \sum_{j=1}^{m}\rho_{p(j)}\frac{f_{p(j)}}{f_c'}; \qquad if \;\; \varepsilon_b > 0 \tag{25}$$

where ε_b is the strain at bottom outermost fiber of the PPC section and can be calculated as follows:

$$\varepsilon_b = \varepsilon_t - \emptyset_{\text{st}} \tag{26}$$

The value of p_c is checked to be less than a specified tolerance (such as 0.005). If the convergence does not meet that criterion, a new curvature, $(\emptyset_{st})_{new}$ is estimated using Newton-Raphson's method using the following equation, and the above-described process is repeated until convergence is achieved.

$$(\emptyset_{st})_{new} = (\emptyset_{st})_{old} - \frac{p_c}{dp_c/d(\emptyset_{st})_{old}} \tag{27}$$

where the derivative $dp_c/d(\emptyset_{st})_{old}$ is calculated using following equations:

$$\frac{dp_c}{d(\emptyset_{st})_{old}} = -\frac{1}{(\emptyset_{st})_{old}{}^2}\left(A\ \frac{\varepsilon_t^5}{5} + B\ \frac{\varepsilon_t^4}{4} + C\ \frac{\varepsilon_t^3}{3} + D\ \frac{\varepsilon_t^2}{2}\right) + \sum_{i=0}^{n}\frac{dp_{st(i)}}{(\emptyset_{st})_{old}} + \sum_{j=0}^{m}\frac{dp_{p(j)}}{d(\emptyset_p)_b}\ ; \qquad if\ \ \varepsilon_b \le 0 \tag{28}$$

$$\frac{dp_c}{d(\emptyset_{st})_{old}} = -\frac{1}{(\emptyset_{st})_{old}{}^2}\left[\frac{A}{5}(\varepsilon_t^5 - \varepsilon_b^5) + \frac{B}{4}(\varepsilon_t^4 - \varepsilon_b^4) + \frac{C}{3}(\varepsilon_t^3 - \varepsilon_b^3) + \frac{D}{2}(\varepsilon_t^2 - \varepsilon_b^2)\right] + \sum_{i=0}^{n}\frac{dp_{st(i)}}{d(\emptyset_{st})_{old}} + \sum_{j=0}^{m}\frac{dp_{p(j)}}{d(\emptyset_p)_b}; \qquad if\ \ \varepsilon_b > 0 \tag{29}$$

while, $dp_{st(i)}/d(\emptyset_{st})_{old}$ and $dp_{p(j)}/d(\emptyset_p)_b$ are obtained from the following equations:

$$\begin{cases} \dfrac{dp_{st(i)}}{d(\emptyset_{st})_{old}} = -\alpha_i\dfrac{\rho_{st(i)}E_s}{f_c'}\ ; \quad if\ |\varepsilon_{st(i)}| \le \varepsilon_{yst} & (30) \\ \dfrac{dp_{p(j)}}{d(\emptyset_p)_b} = -\beta_j\dfrac{\rho_{p(j)}E_p}{f_c'}\ ; \quad if\ |\varepsilon_{p(j)}^{total}| \le \varepsilon_{yp} & (31) \end{cases} \quad \text{Elastic state;}$$

$$\begin{cases} \dfrac{dp_{st(i)}}{d(\emptyset_{st})_{old}} = 0\ ; \quad if\ |\varepsilon_{st(i)}| > \varepsilon_{yst} & (32) \\ \dfrac{dp_{p(j)}}{d(\emptyset_p)_b} = 0\ ; \quad if\ |\varepsilon_{p(j)}^{total}| > \varepsilon_{yp} & (33) \end{cases} \quad \text{Elasto-Plastic state;}$$

where α_i is the distance between the ith steel layer and the top edge of the section and β_j is the distance between the jth prestressing strand layer and the top edge of the section.

Eventually, the ultimate moment capacity (m_0) of the PPC section in the absence of axial force is obtained from the following equations:

$$m_0 = \frac{1}{(\emptyset_{st})_{new}{}^2}\left(A\ \frac{\varepsilon_t^6}{6} + B\ \frac{\varepsilon_t^5}{5} + C\ \frac{\varepsilon_t^4}{4} + D\ \frac{\varepsilon_t^3}{3}\right) + \frac{1}{(\emptyset_{st})_{new}}\sum_{i=1}^{n}\rho_{st(i)}\frac{f_{st(i)}}{f_c'} + \frac{1}{(\emptyset_p)_b}\sum_{j=1}^{m}\rho_{p(j)}\frac{\varepsilon_{p(j)}^{total}f_{p(j)}}{f_c'}; \qquad if\ \ \varepsilon_b \le 0 \tag{34}$$

$$m_0 = \frac{1}{(\emptyset_{st})_{new}{}^2}\left[\frac{A}{6}(\varepsilon_t^6 - \varepsilon_b^6) + \frac{B}{5}(\varepsilon_t^5 - \varepsilon_b^5) + \frac{C}{4}(\varepsilon_t^4 - \varepsilon_b^4) + \frac{D}{3}(\varepsilon_t^3 - \varepsilon_b^3)\right]$$

$$+\frac{1}{(\emptyset_{st})_{new}}\sum_{i=1}^{n}\rho_{st(i)}\frac{f_{st(i)}}{f_c'} + \frac{1}{(\emptyset_p)_b}\sum_{j=1}^{m}\rho_{p(j)}\frac{\varepsilon_{p(j)}^{total} f_{p(j)}}{f_c'}; \qquad if \quad \varepsilon_b > 0 \tag{35}$$

In addition to the key points, a set of points in compression and tension failure regions are presented in Figure 4. The values of $\emptyset_{st}$ and $\emptyset_p$ are decreased by the specified amounts $0.95(\emptyset_{st})_b$ and $0.95(\emptyset_p)_b$ respectively, to get a set of points in the compression failure region; getting a set of points in tension failure region involves increasing $\emptyset_{st}$ and $\emptyset_p$ by the specifiedamounts $1.05(\emptyset_{st})_b$and $1.05(\emptyset_p)_b$, respectively. Subsequently, a third degree polynomial that includes four constants is fitted to the points (m_u,p_u) using the least square method to generate the 2D yield surfaces around the major and minor axes of the PPC section, as follows (Thanoon et al., 2004):

$$\frac{m_{zu}}{m_{z0}} = a_1 + a_2\left(\frac{p_u}{p_0}\right) + a_3\left(\frac{p_u}{p_0}\right)^2 + a_4\left(\frac{p_u}{p_0}\right)^3 \tag{36}$$

$$\frac{m_{yu}}{m_{y0}} = b_1 + b_2\left(\frac{p_u}{p_0}\right) + b_3\left(\frac{p_u}{p_0}\right)^2 + b_4\left(\frac{p_u}{p_0}\right)^3 \tag{37}$$

where subscripts ‘z’ and ‘y’ denote the major and minor axes of the PPC section, respectively; m_u is the moment corresponding to the axial force (p_u). a_1, a_2, a_3 ,a_4; and b_1, b_2, b_3, b_4 are the polynomial constants about the z and y axes, respectively, which are determined by the least square method; m_{zo} and m_{y0} are the dimensionless ultimate moment capacity of the PPC section about major and minor axes, respectively, when the axial force is zero. Finally, the approximate 3D yield surface of the PPC section is depicted in Figure 6. The developed 3D yield surface is essential to perform 3D nonlinear analysis of PPC structures under static and dynamic loads. In this study, 3D yield surface curves have been used to determine the formation of plastic hinges in the PPC sections. Therefore, a plastic hinge is formed when the force state in the PPC element exceeds the yield surface domain, which is the ratio of the applied force to the ultimate capacity. The force/stress state is considered to evaluate the plasticity condition in the element during loading. This force/stress state can be in tension, compression, or shear which affect the section’s failure mode.

2.2. Development of the constitutive law and the FE model for PPC elements

The developed stiffness and constitutive law for PPC frame element can be derived as a combination of a two-noded, 3D inelastic RC frame element and prestressing tendon element, as shown in equation (38). The inelastic stiffness matrix for the RC frame element, derived by Thanoon et al. (2004) using bending theory for small transverse displacements. The elastic stiffness matrix of the prestressing tendon (K_T) is derived by using a two-noded 3D truss element limited to small strain and rotations, as presented in equation (39).

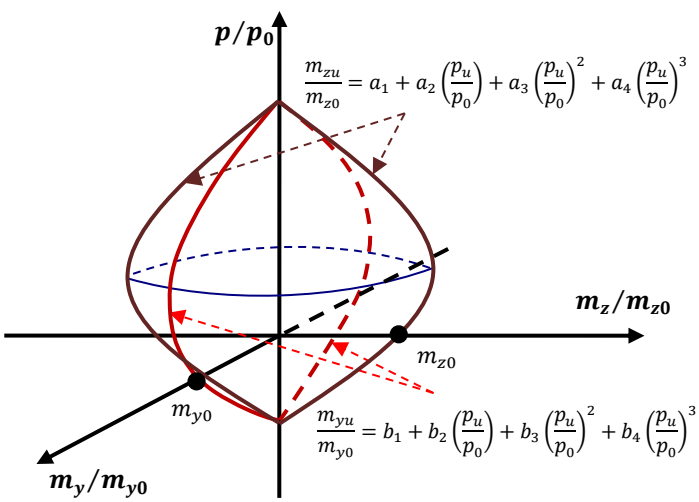

Fig. 6. Three-dimensional yield surface for PPC frame section

Where E_T is the elastic modulus (or reduced elastic modulus if material goes into inelastic range) obtained at the local constitutive relation; l and A_T are the element length and cross sectional area of the prestressed tendon, respectively. Eventually, the final elastic stiffness matrix $(K_{PPC})_e$ of the PPC frame element in the local coordinate system is given in the form of symmetric matrix equation (40).

By considering the lumped plasticity model concepts (Saatcioglu, 1984; Al-Bermani and Kitipornchai, 1990), the elasto-plastic stiffness matrix $(K_{PPC})_{ep}$ of the PPC beam-column element with plastic hinges at one or both ends can be written as:

$$(\mathrm{K_{PPC}})_{\mathrm{ep}} = (\mathrm{K_{PPC}})_{\mathrm{e}} - (\mathrm{K_{PPC}})_{\mathrm{p}} \tag{41}$$

$$[(K_{PPC})_e]_{12x12} = \begin{bmatrix} \vdots & \begin{matrix} \cdots \\ K_{RC} \\ \cdots \end{matrix} & \vdots \end{bmatrix}_{12x12} + \begin{bmatrix} \vdots & \begin{matrix} \cdots \\ K_T \\ \cdots \end{matrix} & \vdots \end{bmatrix}_{12x12}$$

{RC element} {Tendon element}

(38)

$$K_T = \int_0^l E_T A_T B_T^T B_T dx = \frac{E_T A_T}{l} =$$

$$\begin{bmatrix} 1 & 0 & 0 & 0 & 0 & 0 & -1 & 0 & 0 & 0 & 0 & 0 \\ 0 & 0 & 0 & 0 & 0 & 0 & 0 & 0 & 0 & 0 & 0 & 0 \\ 0 & 0 & 0 & 0 & 0 & 0 & 0 & 0 & 0 & 0 & 0 & 0 \\ 0 & 0 & 0 & 0 & 0 & 0 & 0 & 0 & 0 & 0 & 0 & 0 \\ 0 & 0 & 0 & 0 & 0 & 0 & 0 & 0 & 0 & 0 & 0 & 0 \\ 0 & 0 & 0 & 0 & 0 & 0 & 0 & 0 & 0 & 0 & 0 & 0 \\ -1 & 0 & 0 & 0 & 0 & 0 & 1 & 0 & 0 & 0 & 0 & 0 \\ 0 & 0 & 0 & 0 & 0 & 0 & 0 & 0 & 0 & 0 & 0 & 0 \\ 0 & 0 & 0 & 0 & 0 & 0 & 0 & 0 & 0 & 0 & 0 & 0 \\ 0 & 0 & 0 & 0 & 0 & 0 & 0 & 0 & 0 & 0 & 0 & 0 \\ 0 & 0 & 0 & 0 & 0 & 0 & 0 & 0 & 0 & 0 & 0 & 0 \\ 0 & 0 & 0 & 0 & 0 & 0 & 0 & 0 & 0 & 0 & 0 & 0 \end{bmatrix}$$

(39)

$$[(K_{PPC})_e]_{12x12} =$$

$$\begin{bmatrix} \frac{EA}{L}+\frac{E_tA_t}{L_t} & 0 & 0 & 0 & 0 & 0 & -\frac{EA}{L}-\frac{E_tA_t}{L_t} & 0 & 0 & 0 & 0 & 0 \\ 0 & \frac{12EI_z}{c^3} & 0 & 0 & 0 & \frac{6EI_z}{c^3}(2a+c) & 0 & \frac{-12EI_z}{c^3} & 0 & 0 & 0 & \frac{6EI_z}{c^3}(2b+c) \\ 0 & 0 & \frac{12EI_y}{c^3} & 0 & \frac{-6EI_y}{c^3}(2a+c) & 0 & 0 & 0 & \frac{-12EI_y}{c^3} & 0 & \frac{-6EI_y}{c^3}(2b+c) & 0 \\ 0 & 0 & 0 & \frac{GI_x}{L} & 0 & 0 & 0 & 0 & 0 & \frac{-GI_x}{L} & 0 & 0 \\ 0 & 0 & \frac{-6EI_y}{c^3}(2a+c) & 0 & \frac{12EI_y}{c^3}(a+c)a+\frac{4EI_y}{c} & 0 & 0 & 0 & \frac{-6EI_y}{c^3}(2a+c) & 0 & \frac{6EI_y}{c^3}(2ab+c(a+b))+\frac{2EI_y}{c} & 0 \\ 0 & \frac{-6EI_z}{c^3}(2a+c) & 0 & 0 & 0 & \frac{12EI_z}{c^3}(a+c)a+\frac{4EI_z}{c} & 0 & \frac{-6EI_z}{c^3}(2a+c) & 0 & 0 & 0 & \frac{6EI_z}{c^3}(2ab+c(a+b))+\frac{2EI_z}{c} \\ -\frac{EA}{L}-\frac{E_tA_t}{L_t} & 0 & 0 & 0 & 0 & 0 & \frac{EA}{L}+\frac{E_tA_t}{L_t} & 0 & 0 & 0 & 0 & 0 \\ 0 & \frac{-12EI_z}{c^3} & 0 & 0 & 0 & \frac{-6EI_z}{c^3}(2a+c) & 0 & \frac{12EI_z}{c^3} & 0 & 0 & 0 & \frac{-6EI_z}{c^3}(2a+c) \\ 0 & 0 & \frac{-12EI_y}{c^3} & 0 & \frac{6EI_y}{c^3}(2a+c) & 0 & 0 & 0 & \frac{12EI_y}{c^3} & 0 & \frac{6EI_y}{c^3}(2b+c) & 0 \\ 0 & 0 & 0 & \frac{-GI_x}{L} & 0 & 0 & 0 & 0 & 0 & \frac{GI_x}{L} & 0 & 0 \\ 0 & 0 & \frac{-6EI_y}{c^3}(2b+c) & 0 & \frac{6EI_y}{c^3}(2ab+c(a+b))+\frac{2EI_y}{c} & 0 & 0 & 0 & \frac{6EI_y}{c^3}(2b+c) & 0 & \frac{12EI_y}{c^3}(b+c)b+\frac{4EI_y}{c} & 0 \\ 0 & \frac{6EI_z}{c^3}(2b+c) & 0 & 0 & 0 & \frac{6EI_z}{c^3}(2ab+c(a+b))+\frac{2EI_z}{c} & 0 & \frac{-6EI_z}{c^3}(2b+c) & 0 & 0 & 0 & \frac{12EI_z}{c^3}(b+c)b+\frac{4EI_z}{c} \end{bmatrix}$$

(40)

where $(K_{PPC})_p$ is the plastic stiffness and represents the loss of the elastic stiffness due to the development of plastic hinge at one or both ends of beam-column element as presented in equation (42).

$$(\mathrm{K_{PPC}})_\mathrm{p} = (\mathrm{K_{PPC}})_\mathrm{e}.\,\mathrm{G}.\,[G^T.\,(\mathrm{K_{PPC}})_\mathrm{e}.\,\mathrm{G}]^{-1}G^T.\,(\mathrm{K_{PPC}})_\mathrm{e} \tag{42}$$

where $\mathrm{G} = \begin{bmatrix} g_i & 0 \\ 0 & g_j \end{bmatrix}$, and g_i and g_j are the gradient vectors of the yield surface at the both ends of the beam-column element which are dependent on the number of independent stress resultants (Thanoon et al., 2004). The elasto-plastic stiffness matrix of the PPC element is modified after each new occurrence of a plastic hinge. A plastic hinge is assumed to have developed when the position of the nodal force vector (force state) in the PPC element lies on or outside the yield surface domain (Figure 6), which is the ratio of the applied force to the ultimate capacity. In fact, after development of plastic hinges in a PPC structure, the amount of redistributed load on the rest of the elements is increased. Consequently, further plastic hinges occurred in the other structural members by exceeding the force states (p_u, m_u) from the yield surface domains of the sections. The above process is repeated until formation of a failure mechanism in the structure which leads to termination of the analysis (Adeli and Chyou, 1986, 1987; and Adeli and Mabrouk, 1987). Finally, the computational procedure for the developed plasticity theory and constitutive law for the PPC beam-column element were codified and implemented into a finite element program called ARCS3D in the Fortran language (Hejazi et al., 2014, 2016). However, the developed FE algorithm code can be used in any FE structural software for analysis of PPC structures. Figure 7 demonstrates the computation procedure for analysis of PPC structures through the developed FE computer program. This program is validated in this study, as presented below.

3. VALIDATION, VERIFICATION AND RESULTS DISCUSSION

In this paper, the aim of conducting experimental tests is to validate the developed analytical model and plasticity formulation. For this purpose, three full-scale RC and PCC beams and one PPC frame were tested under monotonic bending and lateral pushover loads, respectively, in the structural engineering laboratory of the Putra Malaysia University. Moreover, the results of experimental `test for four story frame building tested by Wei et al. (2012) implemented for comparison with nonlinear dynamic analysis result using developed finite element program in this study as explained in the following sections.

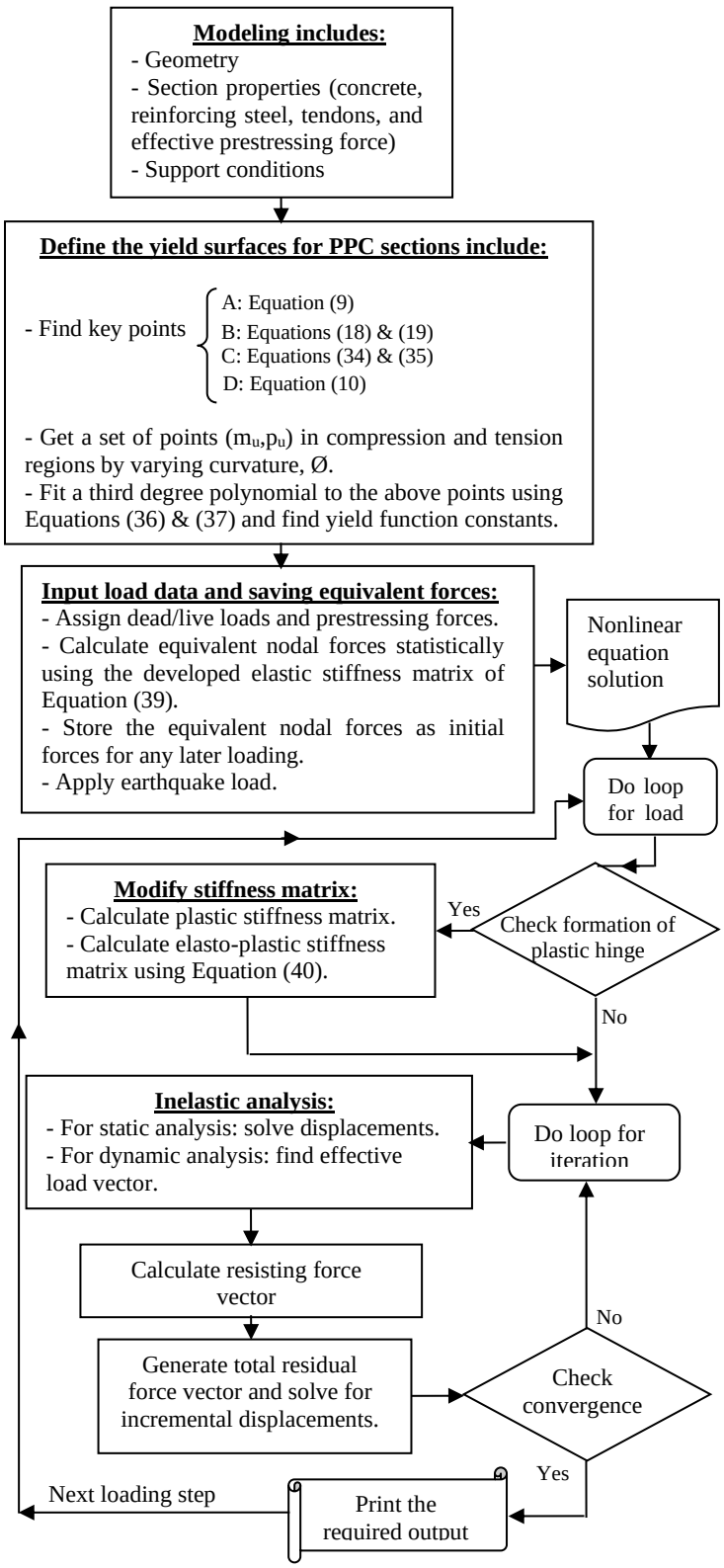

Fig. 7. Computation procedure for analysis of PPC structures in FE program, ARCS3D

3.1. Beam specimens under monotonic bending test

The experimental study of the three simply supported full-scale RC and PPC beams (B1, B2, and B3) was carried out under four-point bending test as shown in Figure 8. The beam specimens were 3 meters long. The first beam (B1) was a conventional RC beam (as a control specimen) shown in Figure 9a. Figures 9b and 9c depict the PPC specimens (B2) and (B3), which include shear stirrups, longitudinal reinforcing steel, and bonded/unbonded prestressed tendons with straight profiles.

Fig. 8. Test setup of beam specimens under four-point bending test

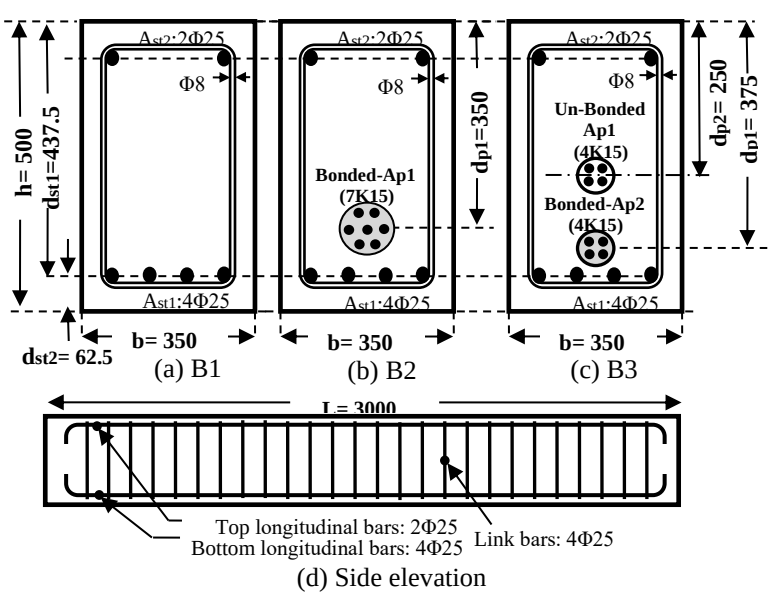

Fig. 9. Dimensional and reinforcement details (units: mm)

For specimen B2, seven-by-seven wire strands (anchorage size: 7K15) of grade 270 ksi (tensile strength, f_{pu}= 1860 MPa) with an area of 980 mm^2 were placed and bonded at a 100 mm eccentricity from the center of specimen B2. For specimen B3, four-by-seven wire strands of grade 270 (anchorage size: 4K15) with an area of 560 mm^2 were placed and bonded at a 125 mm eccentricity from the center of the beam section. In addition, four unbonded grade 270 seven-wire strands were placed at the center of specimen B3.

British code (BS5328, 1997) was used to design the mix proportion of concrete grade 40. The actual quantities required for the mix per bag of cement were 0.4: 1: 1.14: 2.49 for water, cement, and fine and coarse aggregates, respectively. A set of three 150 x 150 x 150 mm^3 control concrete cubes were cast for each beam to determine the concrete compression strength. The mean value of the compression strengths (f_c') for the concrete cubes was determined as 39.2 MPa. Material and geometrical characteristics of the beam specimens are summarized in Table 1.

Table 1: Material and geometrical characteristics of the beam specimens

Model No.	***Reinforced concrete***						***Prestressing steel***							
	f_c' (MPa)	$f_{y,st}$ (MPa)	d_{st1} (mm)	d_{st2} (mm)	A_{st1} (mm^2)	A_{st2} (mm^2)	f_{pu} (MPa)	P_{effet} (kN)	f_{pb} (MPa)	d_{p1} (mm)	d_{p2} (mm)	A_{p1} (mm^2)	A_{p2} (mm^2)	f_{pe}/f_{pu}
B1	39.2	460	437.5	62.5	1964	982	-	-	-	-	-	-	-	-
B2	39.2	460	437.5	62.5	1964	982	1860	1092	1450	350	-	980	-	0.6
B3	39.2	460	437.5	62.5	1964	982	1860	1000	1325	375	250	560	560	0.5

In Table 2, PPR is partial prestressing ratio, ω_p/ω_{st} is proportion of prestressing steel to normal steel and $\omega_{st} + \omega_p$ is the combined reinforcement index (Karayannis and Chalioris, 2013). These parameters have been used to describe the extent of partial prestressing in a rectangular structural member, as presented in Table 2.

Table 2: Partial prestressing indices for the beam specimens

Model No.	***Span length (mm)***	L/d_p	***PPR***	ω_p/ω_{st}	$\omega + \omega_p$
B1	2800	-	-	-	0.22
B2	2800	8	0.51	1.04	0.51
B3	2800	7.47	0.52	1.08	0.56

3.1.1. Comparison of numerical results and test data

The load is applied incrementally and experimental tests were terminated once the crack widths at midspan or near support zones exceeded the maximum allowable crack width (w_k= 0.3mm). Later, the RC and PPC beams were modeled in the developed computer model, and a nonlinear static analysis was conducted to predict the flexural behavior of the beams up to failure. A comparison between results of experimental testing and results of analysis using the developed analytical model was carried out and shown in Figure 10 in terms of the load-deflection curves.

As seen in Table 3, the ultimate experimentally applied loads in specimens B1, B2, and B3 are close to the obtained load through numerical analysis. A maximum difference of about 13% was observed between the experimental results and the analytical model responses; this can occur due to differences between constitutive models of materials as well as support conditions since the support slightly displaced during applied pulling and pushing load for experimental testing. From Table 3, the mean value of F_{Num}/F_{Exp} is equal to 0.93 showing a good accuracy between numerical and experimental results. It can be seen from Figure 10, the analytical model responses of specimens B1, B2, and B3 show significantly good agreement with the test data from the initial elastic stage up to peak load. Hence, the reliability of the developed analytical model and plasticity and yielding theory is validated through these results.

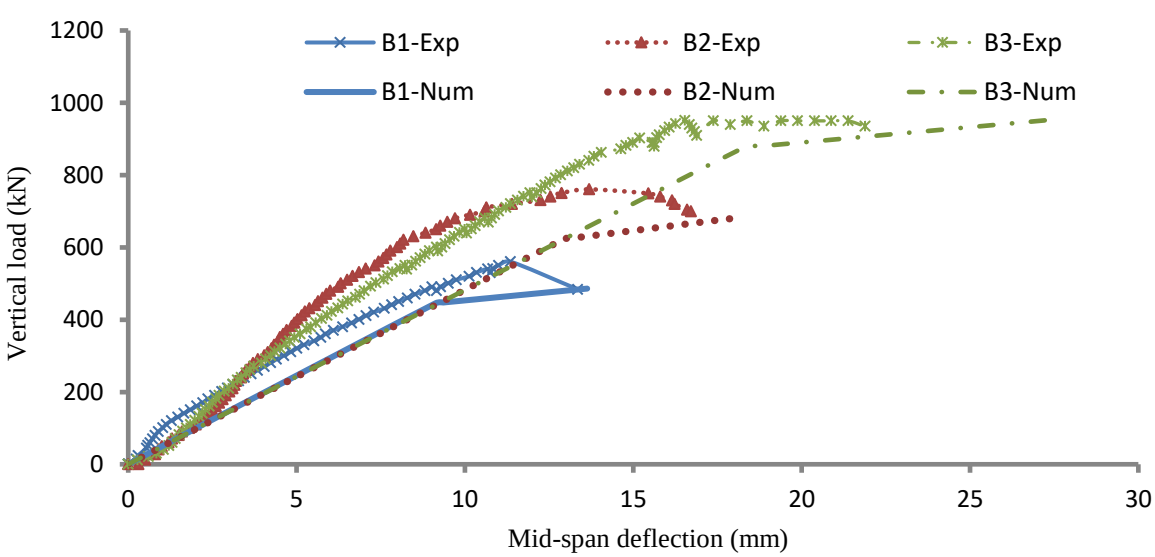

Fig. 10. Load-deflection of experimental tests and numerical predictions for specimens B1, B2 and B3

As seen in Table 3, comparison of the maximum deflections at midspan and the energy capacities (the area under the load-deflection curve) of the simply supported beams shows that the results of the developed analytical model for PPC beam-column elements are quite consistent with the experimental test data. From the details of test specimens in Figure 9, the total non-prestressed steel reinforcement ratios, $\rho_{st,total}$, for all of the beam specimens were the same, and equal to 1.94 percent, and the total prestressed strand ratios, $\rho_{p,total}$, were equal to 0, 0.8, and 0.86 percent for specimens B1, B2, and B3, respectively. However, from experimental tests, the ultimate load capacities of PPC specimens B2 and B3 improved by 35.7 and 70 percent compared to the RC beam (B1). Also, from experimental data, the degree of flexibility (ductility at mid span) of PPC beams B2 and B3 increased by 47.3 and 93.1 percent. Similarly, as shown in Figure 10, significant improvements were observed in both the ultimate load capacity and degree of flexibility of the PPC beam models (B2 and B3) compared to the RC beam model (B1) from the developed numerical models.

A comparison of the RC and PPC beam responses showed that PPC specimen B3 had larger ultimate deflection, higher capacity, and higher energy absorption (area under the load-deflection curves) in comparison with specimens B1 and B2 (Figure 10). This occurred due to the location of the prestressed strands and higher value of PPR, as well as the higher value of ω_p/ω_{st} (Table 2).

Table 3: Comparison of test results and developed analytical model

	Experimental test results			***Analytical model results***			
Beams No.	**Maximum mid-span deflection (mm)**	**Ultimate applied load (F_{exp}) (kN)**	**Area under curve (kN.m)**	**Maximum mid-span deflection (mm)**	**Ultimate applied load (F_{model}) (kN)**	**Area under curve (kN.m)**	**F_{Num}/F_{Exp}**
B1	11.34	560.6	3.8	13.6	486	4.1	0.87
B2	16.7	760.5	8.6	17.9	679.2	7.24	0.90
B3	21.9	951.1	16.53	27.7	955.2	13.70	1.00
Mean	-	-	-	-	-	-	**0.93**

3.1.2. Comparison of results from developed plasticity model with the experimental cracking mechanism

The developed computer model performed the sectional analysis (equations (6)-(35)) for the major (X) and minor (Y) axes to produce a set of points based on the developed plasticity formulation. Subsequently, third

degree polynomials with four constants were fitted to these points, using the least square method to generate mathematical models for the yield surfaces of the section (equations (36) and (37)). The yield function constants and sectional properties of beam specimens B1, B2, and B3 are presented in Table 4. It should be noted that a plastic hinge is formed in a section when the force state (p_u,m_u) in the section either lies outside or on the yield surface.

From the proposed plasticity model (equations (36) and (37)), the axial force-bending moment interaction curves of the RC and PPC frame elements (beam-column sections) in dimensional format are shown in Figure 11. It can be seen in this figure that the PPC beams (B2 and B3) have a slightly lower axial compressive load capacities (key point A in Figure 4) than the RC beam (B1), which is due to the presence of prestressing force. However, as shown in Figures 11a and b, the axial tensile load capacity (point D), the balanced condition (point B), and the ultimate moment capacity (point C) of the PPC members (B2 and B3) have significantly improved compared with the conventional RC member (B1) due to the eccentricity of the tendons and effect of prestressing force.

Table 4: Yield function constants and sectional properties from developed program

	Constant	***B1***	***B2***	***B3***
Coefficient in X-Direction	a_1	1.15764	1.01483	1.02381
	a_2	6.84179	3.97924	3.28645
	a_3	-4.5157	-0.1572	-1.0958
	a_4	-3.3929	-3.9575	-2.3864
Coefficient in Y-Direction	b_1	1.03068	0.86253	0.99075
	b_2	4.32483	2.78763	2.40735
	b_3	-6.0451	-1.0556	-2.1414
	b_4	0.67164	-2.0120	-0.7542
Section properties	P_0 (kN)	6830.3	5992.8	6457.5
	M_{xo} (kN.m)	226.8	317	445.8
	M_{yo} (kN.m)	182.7	244.9	328
	T_0 (kN.m)	197.4	197.4	197.4

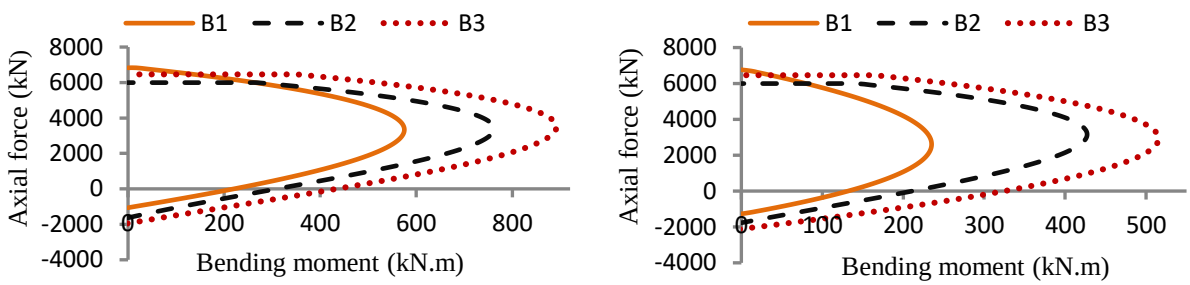

(a) about X-axis (b) about Y-axis

Fig. 11. Axial force-bending moment interaction curves in dimensional format

The 2D yield surface curves of beam-column models B1, B2, and B3 are shown in Figure 12. Figure 12a was obtained by fitting a third degree polynomial (Equation [36]) to a sample of points (p_u,m_{xu}) about the X axis. Similarly, Figure 12b was obtained by fitting a third degree polynomial (Equation [37]) to a sample of points (p_u,m_{yu}) about the Y axis.

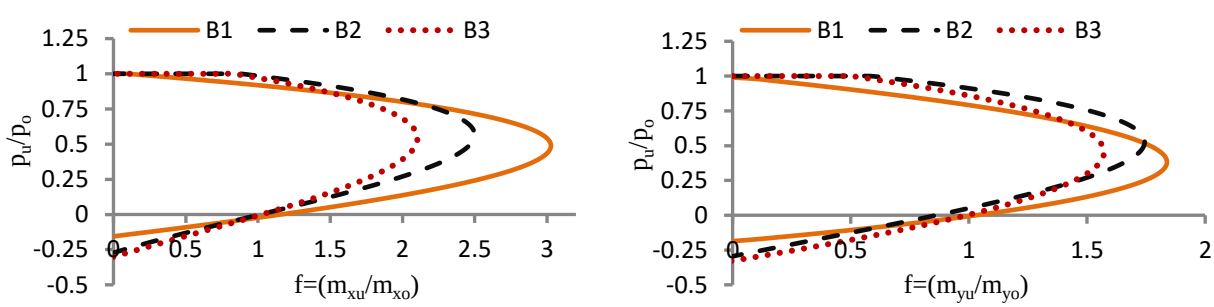

(a) about X-axis (b) about Y-axis

Fig. 12. 2D yield surfaces of the RC and PPC sections

All of the interaction curves of the specimens from numerical analysis were compared with the experimental results to validate and verify the developed plasticity approach, as shown in Figure 13.

From figures 13a-c, the ultimate moment capacities (key point C shown in Figure 4) for B1, B2, and B3 determined via experimental test are close to the results obtained by the numerical model. A maximum difference of 13.3 percent was observed between the experimental result and the mathematical model

predictions for specimen B1. Hence, the developed yielding surface model for the RC and PPC beam-column elements produced results consistent with the experimental testing results.

The cracks in the beam specimens during experimental testing are shown in Figures14a, c and e. The initial cracks were observed at the mid span and applied vertical load zones of the beams. As demonstrated in these figures, by increasing the load, secondary cracks (shear cracks) propagated diagonally near the supports and deep vertical cracks widened at the midspan and reached half way up the cross-section's height due to the high bending value. Forces at initial, secondary and failure cracks of the beams are presented in Table 5.

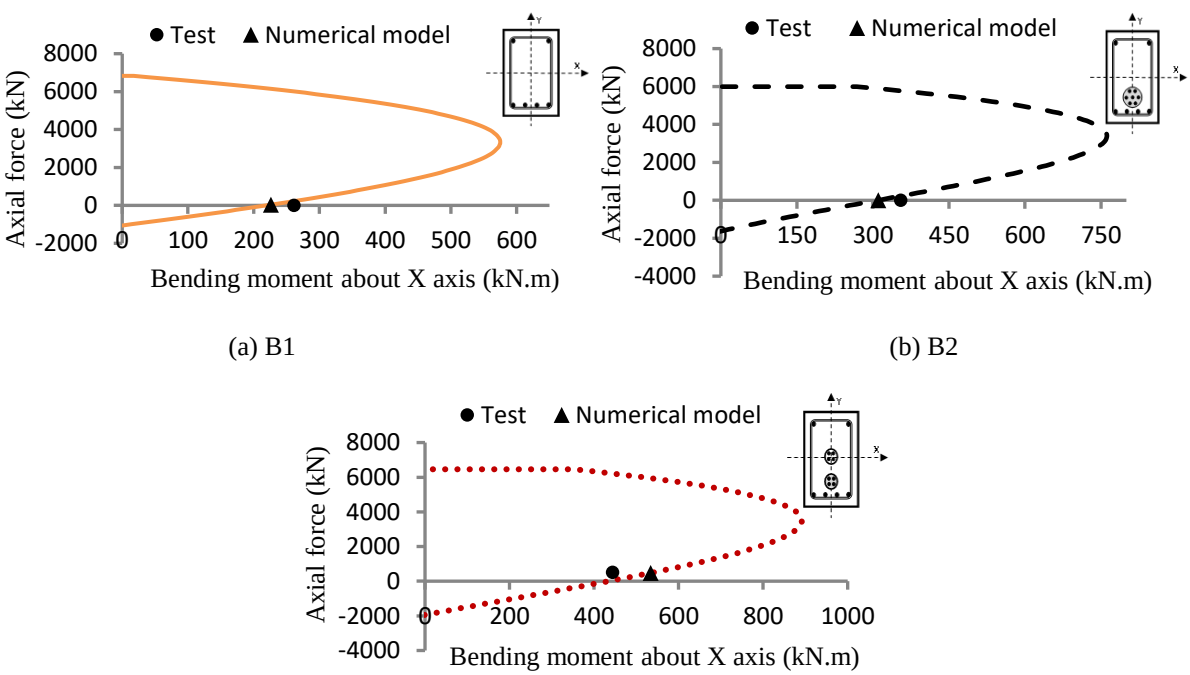

Fig. 13. Comparison of ultimate moment capacities (point C) from mathematical model and test results

It should be noted that small hairy cracks were experimentally observed at the anchorage zones of beams B2 and B3 due to applying effective prestressing forces (P_{effe}) of 1092 kN and 1000 kN, respectively (Table 1). Subsequently, from the developed plasticity model, first and second plastic hinges (preliminary hinges) were formed at the anchorage zones of B2 and B3 models which indicate the presence of high axial force during

prestressing stage (Figures 14d and f). However, the first plastic hinge occurred at the mid span of RC beam model (B1) due to high bending value as shown in Figure 14b.

As seen in Figure 14and Table 5, for beam B2 which was partially prestressed by seven-by-seven wire strands, the initial cracks appeared in the zone of applied vertical loads and at mid-span during the applied force of 370kN, however, the developed computer model determined the initial plastic hinge (damage) in the same zone with force of 396.2 kN, a 6.6% overestimation. Then, by increasing the applied force up to 500kN during experimental test, secondary cracks occurred at the location of applied load same as prediction of computer model but in the force of 461.3kN which indicates7.8% error. Then, the beam failed in force of 760.5kN in experimental test, however, computer model predicted the failure force as 679.2kN with 10% error probably due to considering big load step to reduce computation time. Also, the ultimate moment in the midspan was computed as 317kN.m with 10% variation in compared to the experimental results which is 354.9 kN.

Comparison between test results and computer model predictions for the PPC specimen B3 is shown in Figures 14e and F. Similar to B2, it can be seen that the initial cracks appeared in the zone of applied vertical loads and mid span of B3 once incremental force reached about 270 kN, however, the developed computer model determined the initial plastic hinge in the same zone with force of 318.6kN with 15.2% over estimation. Then, by increasing force up to 951.1 kN during experimental test, the PPC beam failed at the location of applied load same as computer model perditions but in the force of 955.2 kN which indicates less than 0.5% error.

The photo of experimental testing and numerical results of specimen B1 which is conventional reinforced concrete beam and used as benchmark in this study are showed in Figure 14 (a) and (b). As it can be seen in the figure, the initial cracks in experimental test is appeared in middle of beam however by increase of load, the secondary cracks also formed along the beam and then testing is completed by occurring the diagonal failure cracks at end of beam and around the support. The same sequence of plastic hinges formation is predicted through numerical analysis as showed in Figure 14 (b). The applied forces in experimental testing during experience of initial and secondary cracks are measured as 200kN and 265kN respectively. However, these forces in the finite element analysis are predicted by 29% and 14% error as 283kN and 310kN respectively which the difference is due to implementing constitutive model for Concrete Grade 30 in the computer model, though, in this study concrete grade 40 has been used.

However, in this section, the main concern is verification of developed damage plasticity model for PPC concrete and the conventional concrete beam is used as benchmark to compare the behavior only.

Eventually, comparison of the computer model and experimental results indicates that the location of plastic hinge formations and the corresponding load to each plastic hinge determined by proposed constitutive model and plasticity model for PPC element are in a good agreement with the results obtained through experimental tests.

Table 5: Comparison of failure modes between experimental tests and computer model results

	Experimental test results				***Developed computer model Code***				
Beams No.	**Force at first crack (kN)**	**Force at secondary cracks (kN)**	**Force at failure crack (kN)**	**Ultimate moment at midspan (kN.m)**	**Number of plastic hinges**	**Force at first initial hinge (kN)**	**Force at secondary hinges (kN)**	**Force at last hinge (kN)**	**Ultimate moment at midspan (kN.m)**
B1	200	265	560.6	261.1	5	283.5	310	486	226.8
B2	370	500	760.5	354.9	7	396.2	461.3	679.2	317
B3	270	400	951.1	443.9	8	318.6	534.8	955.2	445.8

3.2. Three dimensional PPC framed buildings

3.2.1. Single-bay one-story PPC frame subjected to pushover load

In order to verify the developed numerical model and computer model, a single-bay, one-story PPC frame was casted and tested experimentally under pushover load using dynamic actuator as the details of frame, sections geometry, reinforcements size and arrangements are shown in Figures 15a and b. Also, the finite element modeling of the PPC frame using the developed computer model (ARCS3D program) is demonstrated in Figure 15c. Incremental load with rate of 5.0 mm/min was used in this study. In order to show the effect of PPC element clearly, a distributed load of 1.94 kN/m was applied on the top of the frame in both the experimental and computer models (FE models). Self-weight of the PPC beam was calculated as 0.96 kN/m.

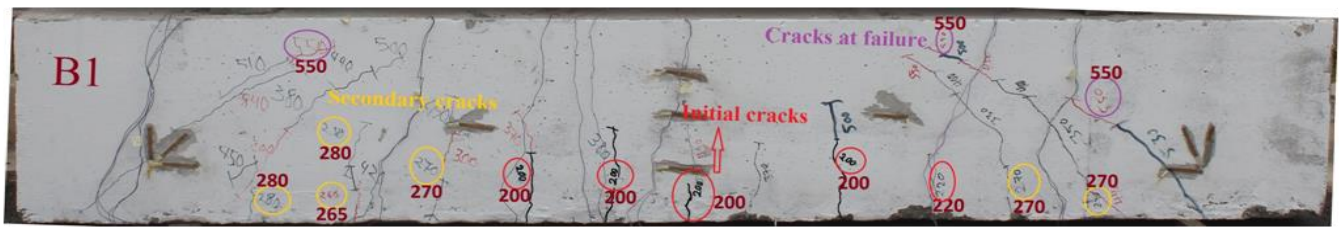

(a) Crack pattern of beam specimen B1 from experimental test

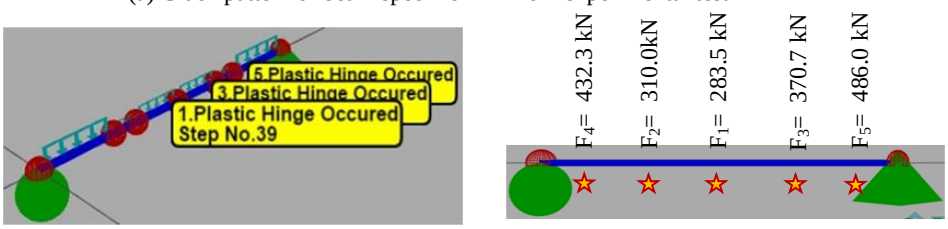

(b) Location and sequence of plastic hinge formations in B1from developed computer model

(c) Crack pattern of beam specimen B2 from experimental test

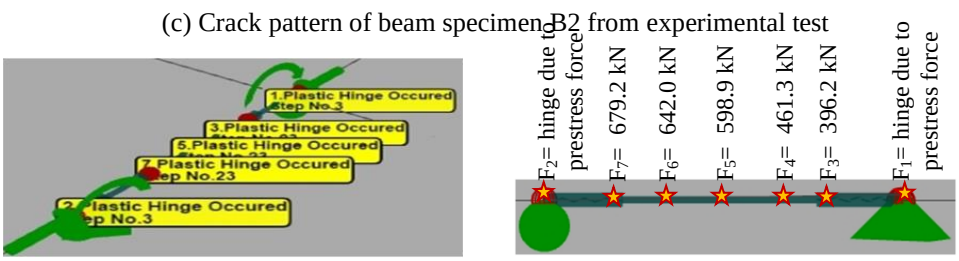

(d) Location and sequence of plastic hinge formations in B2 from developed computer model

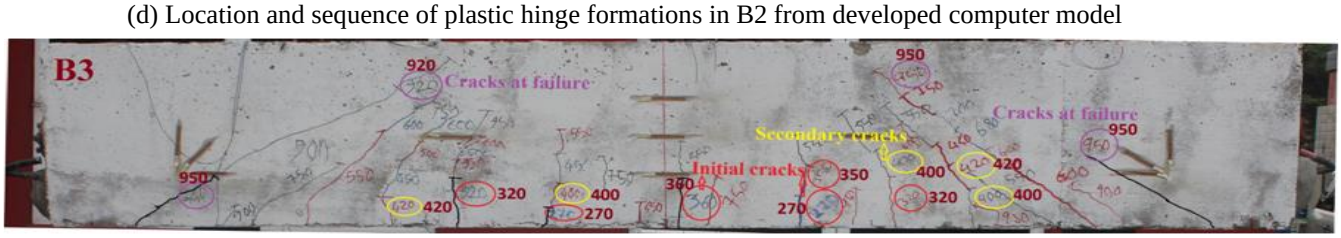

(e) Crack pattern of beam specimen B3 from experimental test

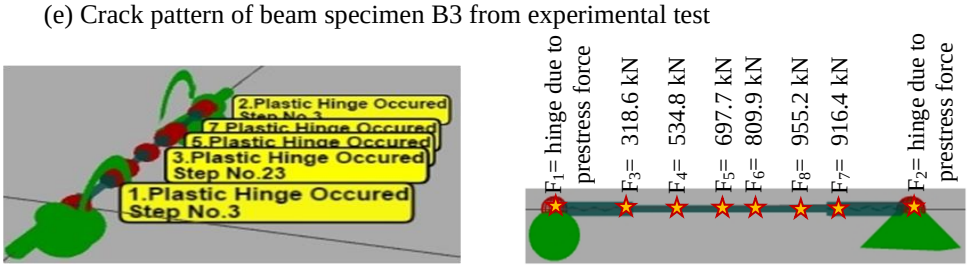

(f) Location and sequence of plastic hinge formations in B3 from developed computer model

Fig. 14. Comparison of crack propagation with the location and sequence of plastic hinges

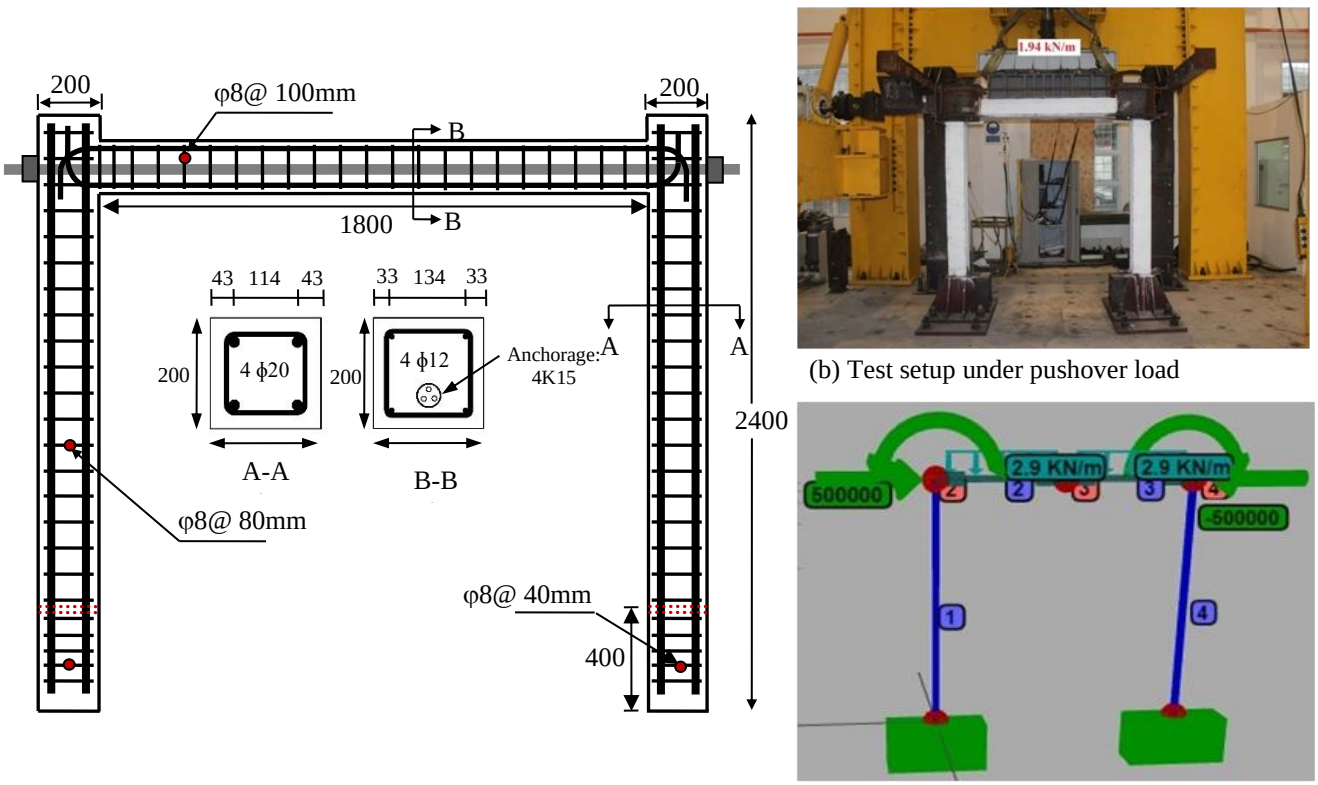

(a) Dimensional and reinforcement details (in mm)

(b) Test setup under pushover load

(c) FEM modeling

Fig. 15. Single-bay one-story PPC frame

Figure 16 indicates the pushover curves obtained from the experimental test and numerical model. From this figure, a slight difference observed between Pushover curves at initial loading stage that would be occurred due to differences between constitutive models of materials as well as minor slip at supports during experimental testing of PPC frame (as mentioned before, there was a bit frame support sliding during experimental testing). From this figure, the maximum lateral load and corresponding displacement are experimentally measured as 63.5 kN and 60.1 mm, respectively. However, it can be seen that the maximum lateral load and corresponding displacement from the numerical model are equal to 62 kN and 66.1 mm, respectively. Moreover, energy dissipation capacities (area under the pushover curves) of 3.9 kN.m and 4.3 kN.m were determined from experimental and numerical observations, respectively. Hence, the comparisons between numerical model predictions and test results demonstrate the reliability of the proposed plasticity model and computer model.

Crack pattern in the beam, column and beam-column joints of the PPC frame is illustrated in Figures17. From Figure 17c, it can be seen that the first was observed at the right beam-column joint in a load of about 28 kN.

Further, second crack appeared at the end of the PPC beam in a load of about 33 kN (Figure 17d). As illustrated in Figures 17e and f, further cracks occurred at the left and right columns near the fixed supports when pushover force reached 34 kN. Subsequently, the fifth and sixth cracks appeared at the left and right beam-column joints of the PPC frame in loads of about 35 kN and 36 kN, respectively. As Figure 17a shows, no crack observed at the midspan zone of the beam component due to presence of prestressing force.

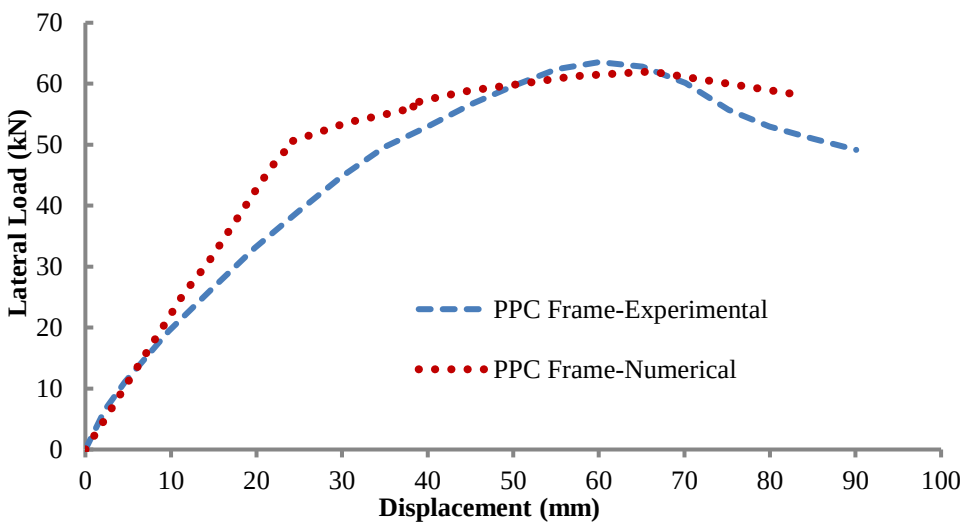

Fig.16. Pushover load-displacement curves of PPC frame

The location and sequence of plastic hinge formations in PPC frame determined by computer model is demonstrated in Figure 17g. As shown in this figure, the lateral pushover load applied to the node 2 and was gradually increased (5 mm/min) until failure of PPC frame model. During FEM analysis, the inelastic seismic pushover analysis terminates when the yield points (plastic hinges) lead to instability of the structure. As it can be seen from Figure 17g and Table 6, the first and second plastic hinges were formed in the beam-column joints near the nodes 4 and 2 at loads about 30.6 kN and 33.2 (load steps 12 and 13), respectively. Later, the third and fourth plastic hinges were formed in both fixed supports at nodes 1 and 5 at loads about 35.7 kN and 38.3 kN (load steps 38 and 39). Table 6 compares the first fifth occurrences of cracks and plastic hinges in terms of forces and corresponding displacements at top of the frame.

A comparison between experimental and computer model results of the PPC frame subjected to pushover load indicates an excellent agreement between crack pattern and location and force of plastic hinges.

Table 6: Comparison of failure modes between experiment and FE results for PPC frame

Damage No.	*Experimental results*		*FE results*	
	Force (kN)	Displacement (mm)	Force (kN)	Displacement (mm)
1st	28	16.1	30.6	14.4
2nd	33	19.8	33.2	15.6
3rd	34	20.3	35.7	16.7
4th	34	20.3	38.3	17.9
5th	35	20.5	40.8	19.1

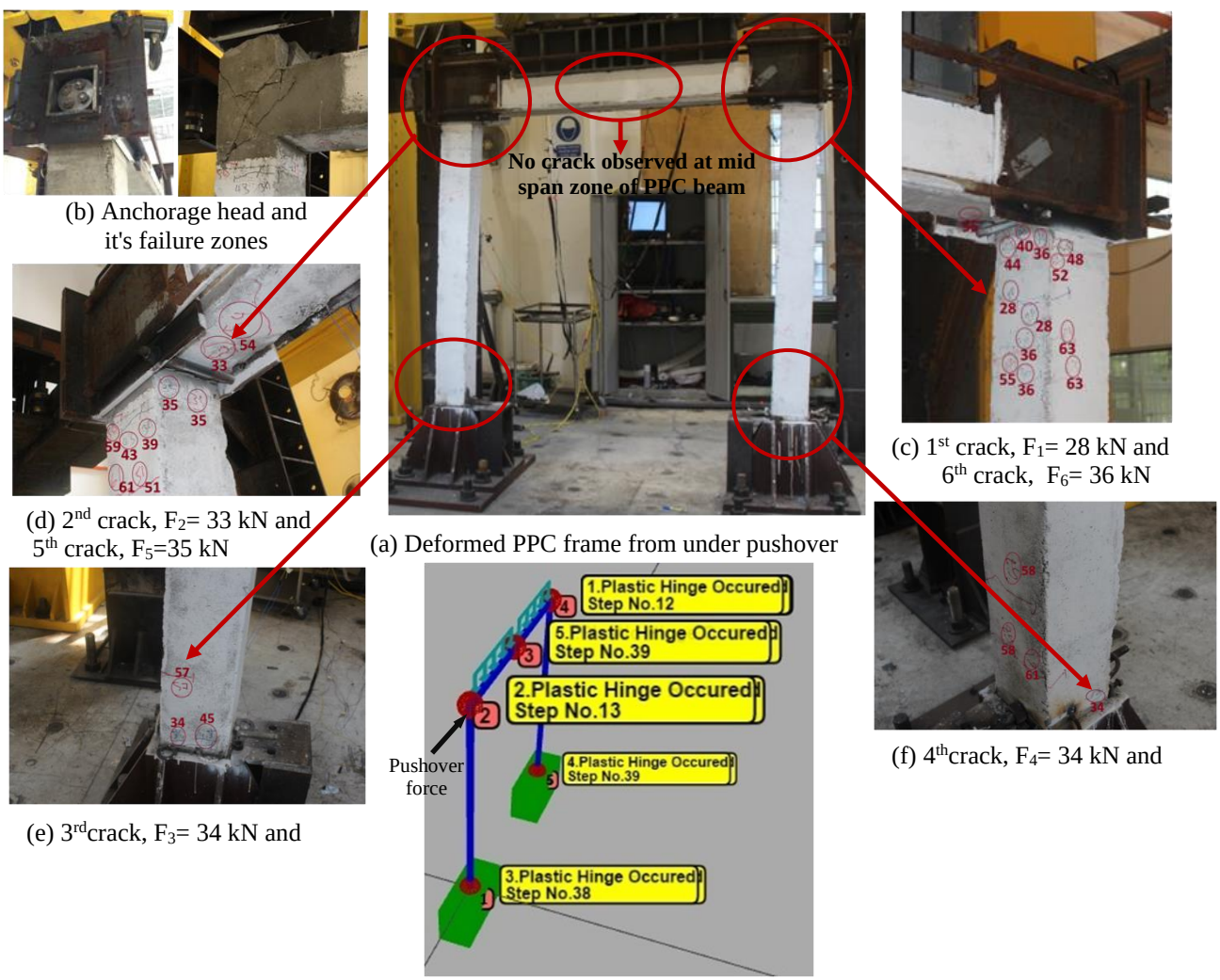

(a) Deformed PPC frame from under pushover

(b) Anchorage head and it's failure zones

(c) 1st crack, F_1= 28 kN and 6th crack, F_6= 36 kN

(d) 2nd crack, F_2= 33 kN and 5th crack, F_5=35 kN

(e) 3rdcrack, F_3= 34 kN and

(f) 4thcrack, F_4= 34 kN and

(g) Location and sequence of plastic hinge formations in PPC frame from developed FE program

Fig. 17. Comparison of crack propagation with location and sequence of plastic hinges (damage) in PPC frame

3.2.2 Four-story building subjected to earthquake excitation

In order to verify the developed numerical model associated with the developed constitutive law for PPC frame element, a four story frame building which experimentally tested by Wei et al. (2012), as depicted in Figure 18a, has been considered for conducting dynamic nonlinear analysis under the El-Centro earthquake excitation. Figure 18b demonstrates the FE model of the four story frame building (Wei et al., 2012) using the developed PPC frame elements in ARCS3D software. The time history analysis was conducted and comparison of experimental and FE analysis results in terms of crack patterns and sequence of hinge formations was performed. Figure 19a presents the experimental results of crack patterns obtained by Wei et al. (2012) and Figure 19b shows the sequence of plastic hinge formations determined by the developed computer model.

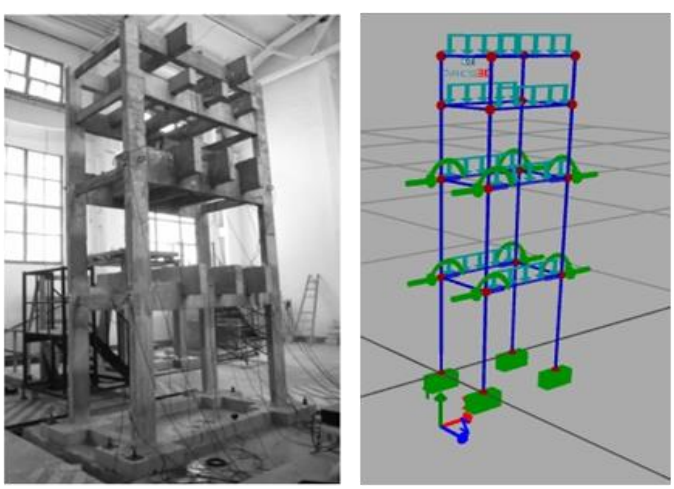

Fig. 18. 3D PPC frame building under El-Centro earthquake (Wei et al., 2012)

Comparison of the Figures 19a and 19b depict that the result of the analytical model developed in the present research is quite consistent with the results of experimental test by Wei et al. (2012). Therefore, the developed analytical model and computer model program code are verified and proven reliable.

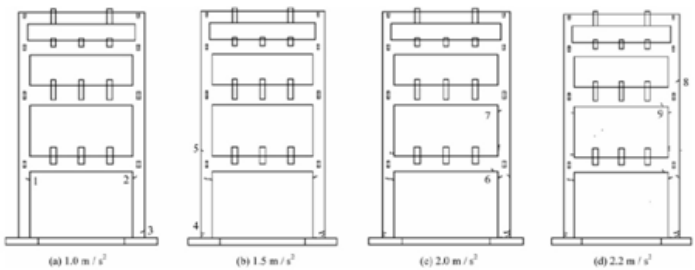

(a) Development of cracks in experimental test (Wei et al., 2012)

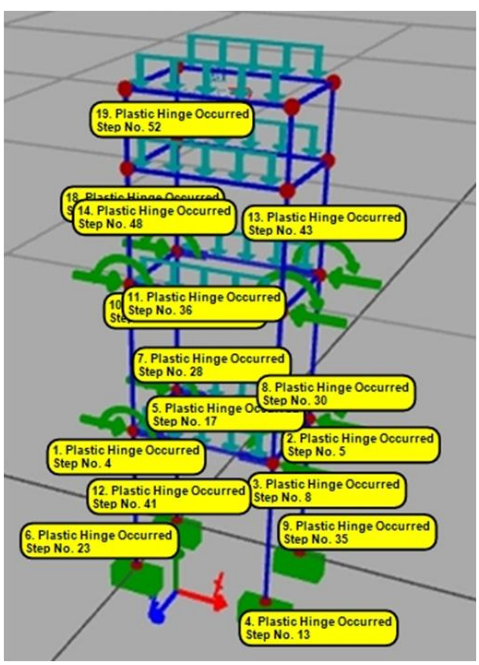

(b) Development of plastic hinges in the developed FE computer program (ARCS3D, 2015)

Fig. 19. Comparison of experimental and FE analysis results in terms of crack patterns and sequence of hinge formations

4 SEISMIC BEHAVIOR OF 3D PPC BUILDING USING DEVELOPED ANALYTICAL MODEL

The developed finite element model is implemented to evaluate seismic response of a multistory RC structure with PPC members and assess the functionality and effects of the PPC frame elements on seismic response of frame. As Figure 20 illustrates, 3D conventional RC and PPC four-story buildings subjected to nonlinear static pushover and dynamic time history analysis were modeled using the developed computer model. The buildings comprised 116 structural elements and 60 nodes distributed in a two-by-three bay-framed model. The bay

widths in the X direction were five, three, and five meters, while the bay widths were three meters long in the Z direction. Each story was considered as three meters high. The buildings were analyzed for extreme amounts of superimposed dead and live loads of 40 kN/m which were assumed to have a uniform distribution load on the beams. The detailed RC column, RC beam, and PPC beam sections are illustrated in Figures 20c to e.

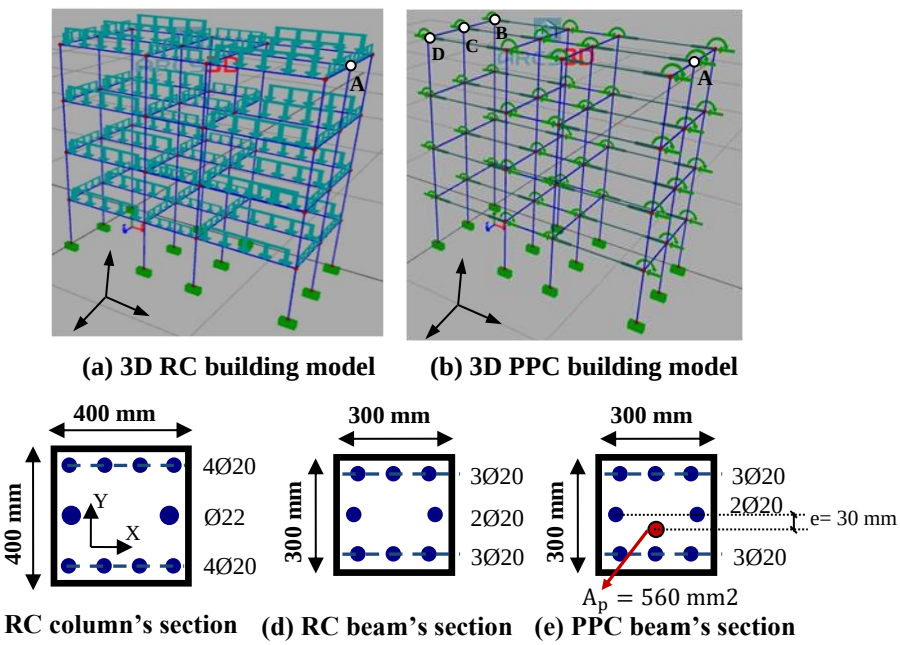

Fig. 20. 3D building models and sectional properties of the RC and PPC beams and columns

The yield strength and Young's modulus of normal reinforcing steel were considered as 400 MPa and 200,000 MPa, respectively. Four-by-seven wire strands of grade 1860 MPa (anchorage size: 4K15 with a diameter of 50 mm) with A_p of 560 mm^2 were placed and bonded at e= 30 mm of the PPC beams, as shown in Figure 20e. The yield strength, Young's modulus, and the equivalent effective prestressing force of tendons were 1860 MPa, 196,500 MPa, and 400 kN, respectively. Fixed support conditions were considered for the columns in contact with the base. Figures 21a and 21b present the axial force-bending moment and 2D yield surface curves of the RC beam and column sections, respectively.

It should be mentioned that the RC sections had the same yield surface curves in the X and Y directions, due to the cross-sections' square geometry and the symmetrical arrangement of the steel bars. However, the yield surface curve in the X direction of the PPC beam section differed from the yield surface curve in the Y direction.

The axial force-bending moment interaction curve and the 2D yield surfaces obtained from the developed plasticity model for the PPC beam section are presented in Figure 22.

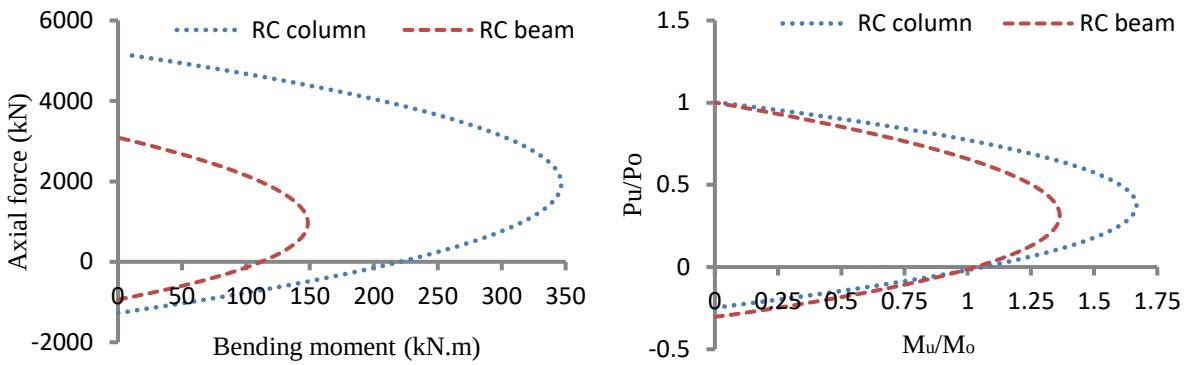

(a) Axial force-bending moment interaction curves (b) 2D yield surfaces

Fig. 21. Interaction curves and 2D yield surfaces of the RC columns and beams

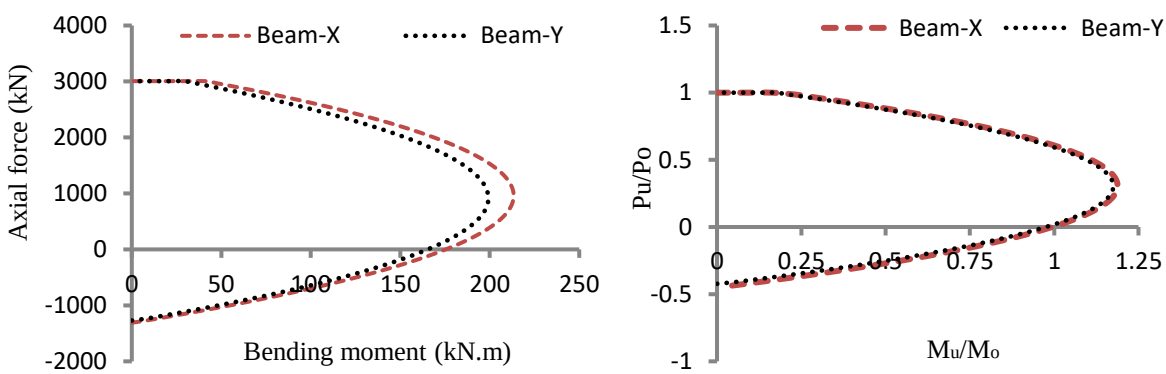

(a) Axial force-bending moment interaction curves (b) 2D yield surfaces

Fig. 22. Interaction curve and 2D yield surface in X and Y directions of the PPC beam

4.1 Nonlinear static pushover analysis

In order to evaluate the effect of PPC element on behavior of frame subjected to the lateral load, two frame are modeled using developed computer model program include of conventional RC frame and RC frame with PPC member, as shown in Figure 20a and 20b respectively.

The pushover monotonic load is applied at nodes ‘B’, ‘C’, and ‘D’ at fourth level of the buildings and after conducting pushover analysis, the load-lateral displacement curves of the four-story RC and PPC buildings which calculated by the developed computer model for node ‘A’ (Figures 20a and b) are shown in Figure 23. As shown in Figure 23, the PPC building exhibited greater stiffness and energy absorption (the area under the curves) due to application of PPC elements which consist of bonded tendons and corresponding prestressing forces. The energy dissipation capacities of the RC and PPC structures were 134.9 kN.m and 197.2 kN.m, respectively which indicating improving the response of the PPC structure by 46.1 percent in comparison to the conventional four-story RC building.

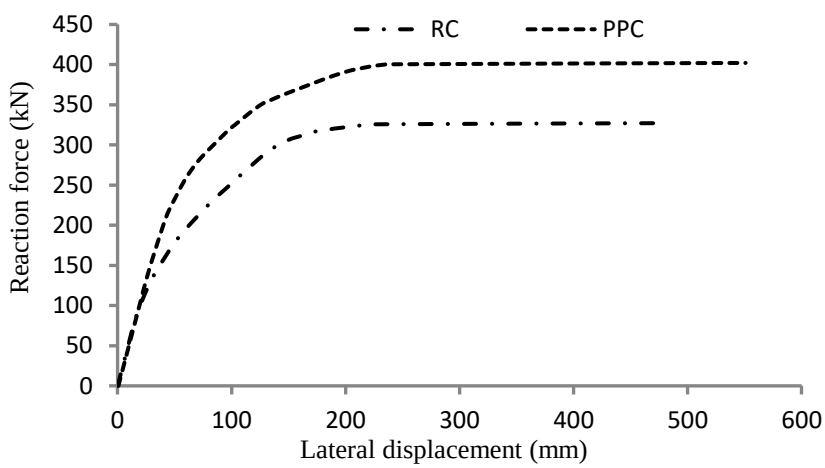

Fig. 23. Comparison of pushover curves of the four-story RC and PPC buildings

4.2 Nonlinear dynamic time history analysis

The seismic analysis of the considered four-storey buildings was conducted by subjecting both model to north-south (X-direction), up and down (Y-direction) and east-west (Z-direction) components of El-Centro earthquake (1940). The time history response of frames for joint ‘A’ which refers to the top node on the fourth floor are shown in Figure 24. The displacement time history results, reveal that the normal and prestressing steels in the PPC elements contributed substantially to the dynamic responses of the concrete structures because of higher capacity and energy absorption and less formation of hinge mechanisms in the frame, as explained in the former section. As showed in Figure 24a, the maximum X-direction positive and negative horizontal

displacements of the four-story RC building subjected to El-Centro earthquake excitations are 29.8 mm (2.16 seconds) and -27 mm (4.53 seconds), respectively.

However, the maximum positive and negative horizontal displacements of the four-story PPC building in the X direction are 16.5 mm and -11.7 mm at 2.31 and 2.15 seconds, respectively. Therefore, the negative lateral displacement of the PPC building in the X direction decreased by 130 percent compared to the RC building. In addition, the positive lateral displacement of the node 'A' in the PPC building in the X direction decreased by 80 percent compared to the RC buildings.

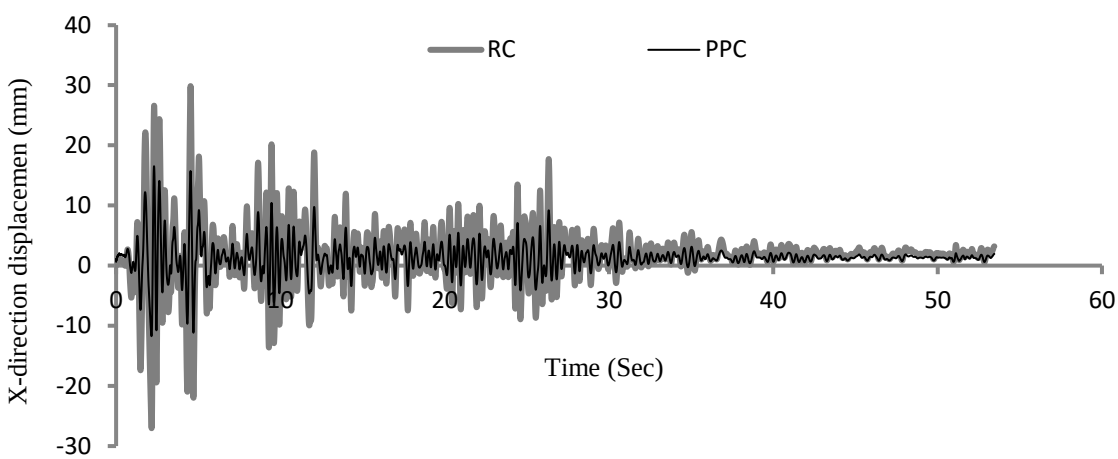

(a) Horizontal displacement at X direction

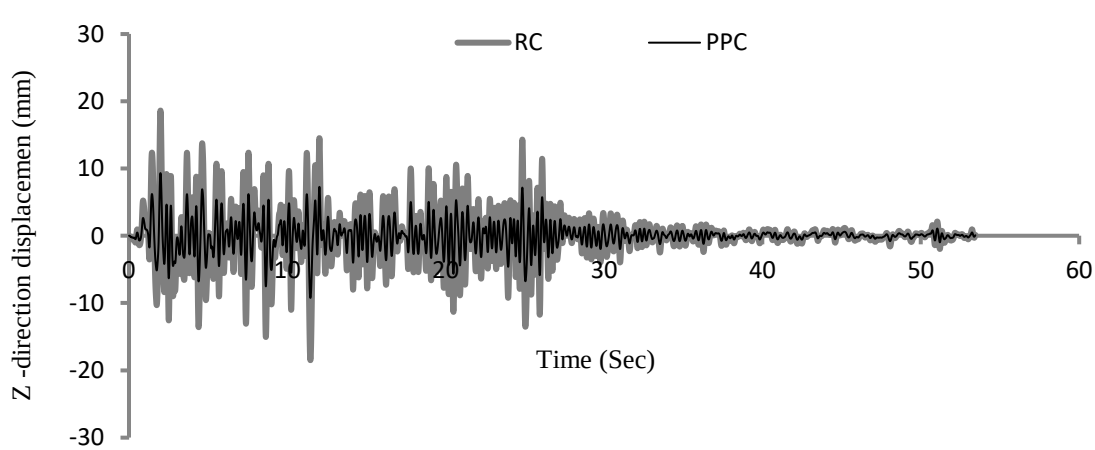

(b) Horizontal displacement at Z direction

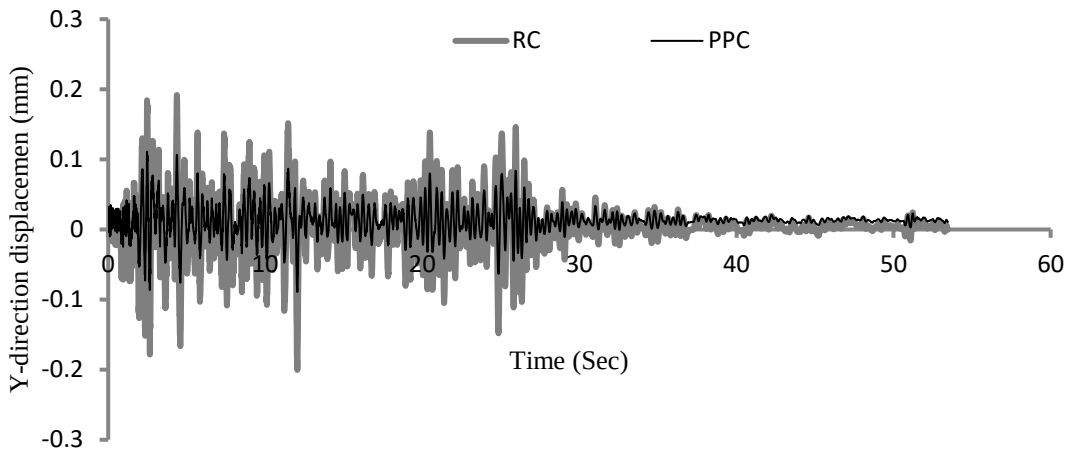

(c) Vertical displacement at Y direction

Fig. 24. Dynamic response of four-story RC and PPC buildings subjected to El-Centro earthquake

As Figure 24b shows, the maximum positive and negative lateral displacements of the PPC building in the Z direction decreased by about 100 percent compared to the RC building. The maximum positive and negative horizontal displacements in the four-story RC in the Z direction are 18.6 mm and -18.5 mm and, for the PPC buildings, are 9.3 mm and -9.2 mm, respectively. Figure 24c illustrates that the four-story RC building had a maximum vertical displacement of about 0.19 mm at 4.37 seconds; however, it was about 0.11 mm at 2.47 seconds in the PPC building. The results of the time history analysis prove that using the PPC elements in long-span buildings increase the damping effect.

The number of plastic hinges formed in the structural components of the four-story PPC building decreased dramatically (by 31.5 percent), reached to 280 plastic hinges, whereas 409 plastic hinges formed in the conventional RC model during applied seismic excitation.

Consequently, the number of plastic hinge formations is significantly reduced in the structural components, especially in the PPC beam elements of considered frame.

5. CONCLUSIONS

The application of the partial prestressing technique has reduced yielding and damages in long-span, light-weight concrete members and structures, and offering an alternative solution to the conventional construction approaches (RC or FPC). However, lack of a comprehensive analytical model capable of identifying damages

in PPC structures under static and dynamic loading is the main challenging issue to conduct nonlinear analysis of RC frames with PPC members. Therefore, this paper aimed to develop a new analytical model for PPC frame elements subjected to static and dynamic loads. For this purpose, the constitutive law and mathematical model for 3 dimensional PPC frame element were formulated. Moreover, to detect damage and to determine the location of plastic hinges formation in the element during dynamic loading, the formulation for plasticity and the yielding surface mechanism for PPC frame element was derived.

The developed analytical model and plasticity model were codified and implemented in a special FEM program of ARCS3D in order to perform inelastic static and dynamic analyses of PPC structures. In order to validate the developed analytical model, plasticity formulation, and the computer model, three conventional RC and PPC beam elements and also a PPC frame were casted and tested experimentally under nonlinear static flexural load and lateral incremental load respectively. A maximum difference of 13% was observed between ultimate load capacities of experimental results and analytical model responses of the beam elements. Further, maximum differences of 9.3%, 2.3% and 9.0% were observed between energy dissipation capacities, maximum lateral loads and corresponding displacements of experimental results and analytical model responses of frames. These may occurred due to differences between constitutive models of materials as well as support condition during experimental. An improvement in constitutive model of concrete in numerical analysis and a perfect support condition during experimental is suggested for future studies.

Also, an experimental seismic testing result for 4 story RC frame with PPC members available in the literature is considered to verify the seismic analysis results by developed computer model. The comparison of all experimental testing data and result of developed analytical model, revealed a good agreement between the numerical simulation and the experimental testing results and demonstrated the reliability of the proposed model.

The experimental and numerical result of beams and frames indicated that although implementing of the prestressing strands increase the construction costs for PPC members but significant improvements were observed in ductility, ultimate failure load, crack control, and energy dissipation capacity compared to the RC beam specimen without increasing the member depth. Also, the number of plastic hinges formed in the frame with PPC member highly decreased in comparison to the conventional RC building.

Ultimately, this study facilitates the analysis and design procedures of multistory PPC and RC buildings and increase the computational efficiency and thereby facilitate the improvement of current design methods.

Declarations

- **Availability of data and material**

  The datasets used and/or analysed during the current study are available from the corresponding author on reasonable request.

- **Competing interests:**

  There is No competing interests.

- **Funding and Acknowledgements:**

  This work received financial support from the Ministry of Higher Education of Malaysia under FRGS Research Project No. 5524748 and received further support from the University Putra Malaysia under Putra Grant No. 9438709. Their support is gratefully acknowledged.

- **Authors' contributions:**

  Farzad Hejazi: Designed experimental test setup, Reviewed and Edited Manuscript

  Milad Hafezolghorani: Design concept of study, developed the methodology, Conducting test, provide info data, process the methodology according to design details, conduct FEM modeling, prepare draft of paper.

  Hojjat Adeli: Technical reviewing and editing

REFERENCES

1. ACI Committee 318. (2005). Building code requirements for structural concrete. American Concrete Institute, Farmington Hills, Detroit, Michigan, USA.
2. Adeli, H. & Chyou, H. (1986), Plastic Analysis of Irregular Frames on Microcomputers. Computers and Structures, 23(2), 233-240.

3. Adeli, H. & Chyou, H. (1987), Microcomputer-Aided Optimal Plastic Design of Frames. Journal of Computing in Civil Engineering, 1(1), 20-34.
4. Adeli, H. and Mabrouk, N. (1986), Optimum Plastic Design of Unbraced Frames of Irregular Configuration. International Journal of Solids and Structures, 22(10), 1117-1128.
5. Agrawal, G., & Bhattacharya, B. (2010). Partial safety factor design of rectangular partially prestressed concrete beams in ultimate flexural limit state. Journal of Structural Engineering, 37(4), 257–267.
6. Al-Bermani, F., & Kitipornchai, S. (1990). Nonlinear analysis of thin-walled structures using least element/member. Journal of Structural Engineering, 116(1), 215–234.
7. Al-Jurmaa, M., & Abdul-Razzak, A. (2009). Analysis of Pretensioned Partially Prestressed Concrete Beams. Researchgate.net, 6(2), 26–32.
8. Alkhairi, F., & Naaman, A. (1993). Analysis of beams prestressed with unbonded internal or external tendons. Journal of Structural Engineering, 119(9), 2680–2700.
9. Amezquita-Sanchez, J. P., & Adeli, H. (2016). Signal Processing Techniques for Vibration-based Health Monitoring of Structures. Archives of Computational Methods in Engineering, 23(1), 1–15.
10. ARCS3D. (2015). Finite elememnt program, Analysis of reinforced concrete structures, Copyright by University Putra, Malaysia.
11. Ariyawardena, N., & Ghali, A. (2002). Prestressing with unbonded internal or external tendons: analysis and computer model. Journal of Structural Engineering, (December), 1493–1501.
12. Au, F. T. K., & Du, J. S. (2004). Partially prestressed concrete. Progress in Structural Engineering and Materials, 6(2), 127–135.
13. Ayoub, A., & Filippou, F. (2009). Finite-element model for pretensioned prestressed concrete girders. Journal of Structural Engineering, 136(4), 401–409.
14. Biritish Standard 5328-2. (1997). Concrete. Methods for specifying concrete mixes.
15. Chern, J., You, C., & Bazant, Z. (1992). Deformation of progressively cracking partially prestressed concrete beams. PCI Journal, 1(37), 74–84.

16. Choudhary, K., & Akhtar, S. (2019). Application of partial prestressing for crack control in reinforced concrete structures. In: AIP Conf Proc, 2158(1). AIP Publishing; 20027.
17. Cohn, M., & MacRae, A. (1984). Prestressing optimization and its implications for design. PCI Journal, 29(4), 68–83.
18. CSA Standard. A23. 3-04. (2004). Design of concrete structures. Canadian Standard Association.
19. Franchetti, P., Modena, C., & Feng, M. Q. (2009). Nonlinear damping identification in precast prestressed reinforced concrete beams. Computer-Aided Civil and Infrastructure Engineering, 24(8), 577–592.
20. Gupta, S., Itoh, Y. and Niwa, J. I. (1994). An Object-Oriented Diagnostic System for Prestressed Concrete Bridges. Computer-Aided Civil and Infrastructure Engineering, 9(6), 385–399.
21. Hejazi, F., Shahpasand, M., Mirnezhad, M., Jaafar, M. S., & Abang Ali, A. A. (2014). A web-based architecture for interactive finite element program. In Computing in Civil and Building Engineering - Proceedings of the 2014 International Conference on Computing in Civil and Building Engineering (pp. 1393–1400).
22. Hejazi, F., Shoaei, M. D., Tousi, A., & Jaafar, M. S. (2016). Analytical Model for Viscous Wall Dampers. Computer-Aided Civil and Infrastructure Engineering, 31(5), 381–399.
23. Hejazi, F., Toloue, I., Jaafar, M. S., & Noorzaei, J. (2013). Optimization of earthquake energy dissipation system by genetic algorithm. Computer-Aided Civil and Infrastructure Engineering, 28(10), 796–810.
24. Hejazi, F., Zabihi, A., & Jaafar, M. S. (2014). Development of elasto-plastic viscous damper finite element model for reinforced concrete frames. Soil Dynamics and Earthquake Engineering, 65, 284–293.
25. Huang, Y. (2012). Finite element method for post-tensioned prestressed concrete structures. PhD Thesis, Department of Engineering, UMI University, Norman, Oklahoma.
26. Hung, S.L. & Adeli, H. (1994), Object-Oriented Back Propagation and Its Application to Structural Design. Neurocomputing, 6(1), 45-55.
27. Karayannis, C. G., & Chalioris, C. E. (2013). Design of partially prestressed concrete beams based on

the cracking control provisions. Engineering Structures, 48, 402–416.

28. Kien, N. D. (2008). Dynamic Response of Prestressed Timoshenko Beams Resting on Two-Parameter Foundation to Moving Harmonic Load. TECHNISCHE MECHANIK, 3(4), 237–258.
29. Laskar, A., Howser, R., Mo, Y., & Hsu, T. (2010). Modeling of Prestressed Concrete Bridge Girders. In Earth and Space 2010, ASCE (pp. 2870–2887).
30. Lei, Y., Zhou, H., & Lai, Z.-L. (2015). A Computationally Compact Algorithm for Real-time Detection of Abrupt Structural Stiffness Degradations. Structural Health Monitoring 2015.
31. Li, S., Zhao, X., & Zhou, G. (2019), Automatic pixel-level multiple damage detection of concrete structure using fully convolutional network. Computer-Aided Civil and Infrastructure Engineering, 34(7), 616-634.
32. Lou, T., Lopes, S. M. R., & Lopes, A. V. (2013). Nonlinear and time-dependent analysis of continuous unbonded prestressed concrete beams. Computers & Structures, 119, 166–176.
33. Medland, I. C., & Taylor, D. A. (1971). Flexural rigidity of concrete column sections. Journal of the Structural Division, 97(2), 573–586.
34. Naaman, A. (1983). An approximate nonlinear design procedure for partially prestressed concrete beams. Computers & Structures, Il(2), 287–299.
35. Naaman, A. E., Harajii, M. H., & Wight, J. K. (1986). Analysis of Ductility in Partially Prestressed Concrete Flexural Members. PCI Journal, 31(3), 64–87.
36. Navarro Gregori, J., Miguel Sosa, P., Fernández Prada, M. a., & Filippou, F. C. (2007). A 3D numerical model for reinforced and prestressed concrete elements subjected to combined axial, bending, shear and torsion loading. Engineering Structures, 29(12), 3404–3419.
37. Oukaili, N. K., & Khattab, M. M. (2019). Serviceability and ductility of partially prestressed concrete beams under limited cycles of repeated loading. Int J. 17:9–15.
38. Ozkul, O. (2007). A new methodology for the analysis of concrete beams prestressed with unbonded tendons. PhD Thesis, Departement of Civil and Environmental Engineering, The State University of New Jersey, USA.
39. Park, R., & Paulay, T. (1975). Reinforced concrete structures. John Wiley & Sons.

40. Preciado, A., Sperbeck, S. T., & Ramírez-Gaytán, A. (2016). Seismic vulnerability enhancement of medieval and masonry bell towers externally prestressed with unbonded smart tendons. Engineering Structures, 122, 50–61.
41. Qarib, H., & Adeli, H. (2014). Recent Advances in Health Monitoring of Civil Structures. Scientia Iranica - Transaction A: Civil Engineering, 21(6), 1733–1742.
42. Recupero, A., D'Aveni, A., & Ghersi, A. (2005). Bending Moment–Shear Force Interaction Domains for Prestressed Concrete Beams. Journal of Structural Engineering, 131(9), 1413–1421.
43. Saatcioglu, M. (1984). Computer-aided aseismic design of reinforced concrete structures. Computer-Aided Analysis and Design of Concrete Structures, 859.
44. Sarma, K. & Adeli, H. (1998), Cost Optimization of Concrete Structures. Journal of Structural Engineering. 124(5), 570-578.
45. Shushkewich, K. (1990). Moment-curvature relationships for partially prestressed concrete beams. Journal of Structural Engineering, 116(10), 2815–2823.
46. Sirca, G. F., & Adeli, H. (2005). Cost optimization of prestressed concrete bridges. Journal of Structural Engineering, 131(3), 380–388.
47. Sirca, G. F., & Adeli, H. (2012). System Identification in Structural Engineering. Scientia Iranica - Transaction A: Civil Engineering, 19(6), 1355–1364.
48. Skogman, B., Tadros, M., & Grasmick, R. (1988). Flexural strength of prestressed concrete members. PCI Journal, 33(5), 96–123.
49. Spinella, N. (2013). N-M-χ interaction for arbitrary cross section under biaxial bending and axial load. Pollack Periodica, 8(3), 87–100.
50. Talaeitaba, S., & Torki, M. (2014). Nonlinear finite element analysis of RC beams under combined shear and torsion to extract linear and curvilinear ranges of interaction curves. SCIENTIA IRANICA, 21(4), 1249–1262.
51. Tanchan, P. (2001). Flexural Behavior of High Strength Concrete Beams Prestressed with Unbonded Tendons. PhD Thesis. The State University of NJ, New Brunswick, NJ.
52. Tang, Y., & Chen, H. (2019). Characterizations on fracture process zone of plain concrete. Journal of

Civil Engineering and Management, 25(8), 819-830.

53. Thanoon, W. a., Paul, D. K., Jaafar, M. S., & Trikha, D. N. (2004). Influence of torsion on the inelastic response of three-dimensional r.c. frames. Finite Elements in Analysis and Design, 40(5-6), 611–628.
54. Wei, W., Zhang, H., & Li. (2012). Seismic performances of large-span prestressed concrete frame structure by shaking table tests. Wuhan University Journal of Natural Sciences, 17(3), 261–267.
55. Xue, W., Tan, Y., & Peng, F. (2020). Experimental Study on Damaged Prestressed Concrete Beams Using External Post-Tensioned Tendons. ACI Structural Journal, 117(1).
56. Yu, G. & Adeli, H. (1993), Object-Oriented Finite Element Analysis Using EER Model. Journal of Structural Engineering, ASCE, 119(9), 2763-2781.
57. Zhang, X., Rajan, D., & Story, B. (2019), Concrete crack detection using context-aware deep semantic segmentation network. Computer-Aided Civil and Infrastructure Engineering, 34(11), 951-971.